AD-A081 858 MASSACHUSETTS INST OF TECH LEXINGTON LINCOLN LAB F/G 21/2
DETECTABILITY OF COLD ROCKET PLUMES.(U)
OCT 79 G F DIONNE, M M LITVAK, J A WEISS F19628-80-C-0002
UNCLASSIFIED TN-1979-48 ESD-TR-79-264 NL

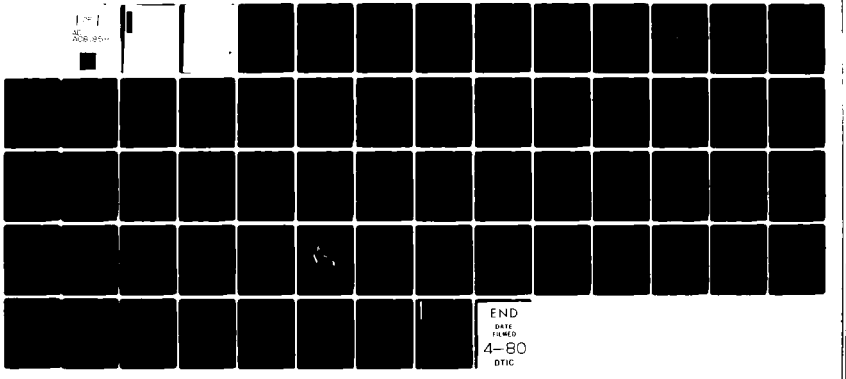

END
DATE FILMED
4-80
DTIC

MASSACHUSETTS INSTITUTE OF TECHNOLOGY

LINCOLN LABORATORY

DETECTABILITY OF COLD ROCKET PLUMES

G. F. DIONNE
M. M. LITVAK
J. A. WEISS
Group 33

W. D. FITZGERALD
Group 34

TECHNICAL NOTE 1979-48

11 OCTOBER 1979

LEXINGTON MASSACHUSETTS

ABSTRACT

The problem of detecting high altitude rocket plumes with satellite-borne submillimeter-wave radiometers is examined from both theoretical and experimental points of view. To estimate the sizes of plume signatures contrasted against a 250-K earth background or in self-emission against the cold sky, a computer program has been developed to predict plume brightness temperatures and optical depths of rotational lines of plume molecular constituents (e.g., H_2O) as a function of distance from the nozzle. The methods employed in the computations are described in general terms, and examples are presented to indicate that detectable H_2O signatures extending to several thousand nozzle diameters should exist at plume altitudes above 250 km. Details of a laboratory water vapor jet operating in a high vacuum environment designed to simulate a rocket plume at high altitude are outlined. Sensitivity considerations relevant to the plume detection problem are discussed for Fourier transform spectrometers and heterodyne receivers designed to study spectral lines in the submillimeter-wave region. Finally, a technique for converting the heterodyne radiometer into a spectrometer is described as a means of obtaining line shape details of the 752-GHz H_2O line.

CONTENTS

I. INTRODUCTION

The possibility of observing high altitude (i.e., above 150 km) plumes of third stage, mid-course vernier, or bus rocket motors from satellites by means of submillimeter-wave heterodyne detectors was discussed in an earlier report (1). Because atmospheric opacity is extremely high in the range of frequencies from 300 to 3000 GHz, satellite detection of rocket launches would not be disrupted by terrestrial radiation, either natural or intended. Other advantages include the possibility of utilizing agile beam electronic scanning techniques, the likelihood of determining altitude and velocity parameters from Doppler shifts of spectral lines, and the benefits associated with the expected low-temperature signature of the plume.

Through the approximately adiabatic expansion which occurs as the rocket effluent expands from the nozzle, rapid cooling creates a large region of low temperature. Surrounding this cold core is an envelope of higher temperature, the air-gas mixing layer, created by collisions between plume gas and atmospheric molecules. This mixing layer region is believed to be relatively transparent at the submillimeter and infrared wavelengths for the high-altitude case. Since some of the low-energy rotational states of the H_2O molecule (a prominent plume constituent) are expected to remain in approximate thermal equilibrium with the adiabatic expansion of the core region, selected spectral lines in this frequency range should be optically thick and colder than the warm earth background.

Under such conditions, radiometry is not only possible within the width of the spectral line, but offers an additional advantage of not being dependent

on the existence of hot portions of the plume, such as the mixing layer. Any attempts to reduce the intensity of the plume infrared radiation by modifying fuel components, for example, would not be expected to decrease the size of the cold signature at submillimeter wavelengths.

In this report, the problem of observing cold rocket plumes from a satellite is examined from two aspects: 1) the temperature, absorptivity (discussed in terms of the optical depth of the spectral line), and size of the plume signature, and 2) the instrumentation required to detect a plume both in laboratory simulations and in the systems application described previously (1).

II. THEORETICAL STUDIES

A. Plume Core Versus Mixing Layer Phenomenology

To describe the high-altitude plume signature theoretically, different sets of calculations are required for typical streamlines that lie along the center of the plume core, on the one hand, or at the inner edge of the mixing layer on the other hand. The plume core is that part of the rocket exhaust gas that flows downstream and is initially unaffected by collisions with the ambient air. The mixing layer is the region surrounding the plume core where ambient air and plume gas mix equally and interact by momentum-changing collisions. Eventually, the plume core is dissipated by these collisions, and the exhaust gas diffuses into the atmosphere a few mean-free paths downstream (2).

The core is expected to be radiationally-thick in the transitions between the low-lying rotational energy levels considered here. The mixing layer should be radiationally-thin in these same transitions. The hot mixing layer is caused by collisions between the plume gas and the ambient air that might be moving past at a relative velocity of about 5 km-s^{-1}. The signal above the earth background originating from the hot mixing layer due to self-emission is not as strong as the signal below the earth background from cold plume core absorption of earth background radiation, in the low-lying rotational transitions. Differing amounts of Doppler-shifting in mixing layer and core further distinguish the two regions in a frequency-resolved spectrum of the plume, whether or not the earth is viewed as background. Plume core self-emission at antenna temperatures ranging between about 50 and 100K, against the cold (2.7 K) sky, is also expected.

The basic structure of a rocket plume at high altitudes is shown in Fig. 1, where the inner core and outer mixing layers appear as distinct regions. The relative velocity $\vec{V}_{12}$ of the two fluids relaxes to small values, comparable to the local thermal speed, in a characteristic mixing layer thickness ℓ_m (in the direction of $\vec{V}_{12}$) given by

$$\ell_m = (V/V_{12}) \frac{m_1+m_2}{\rho_1+\rho_2} \frac{1}{\sigma} \tag{1}$$

where m_1, ρ_1 and m_2, ρ_2 are the mean molecular mass (g/particle) and mass density (g/cm^3) of the ambient air and plume core, respectively, on opposite sides of the mixing layer. The factor σ is the effective momentum-changing collision cross-section (cm^2). The relative velocity

$$\vec{V}_{12} = \vec{V}_1 - \vec{V}_2 \tag{2a}$$

and the mean fluid velocity

$$\vec{V} = (\rho_1\vec{V}_1 + \rho_2\vec{V}_2)/(\rho_1 + \rho_2), \tag{2b}$$

where $\vec{V}_1$ and $\vec{V}_2$ are the fluid velocities on opposite sides of the mixing layer at a point downstream.

The temperature of the mixing layer is calculated from the specific enthalpy h of the mixture, whose stagnation value is the mass average of the

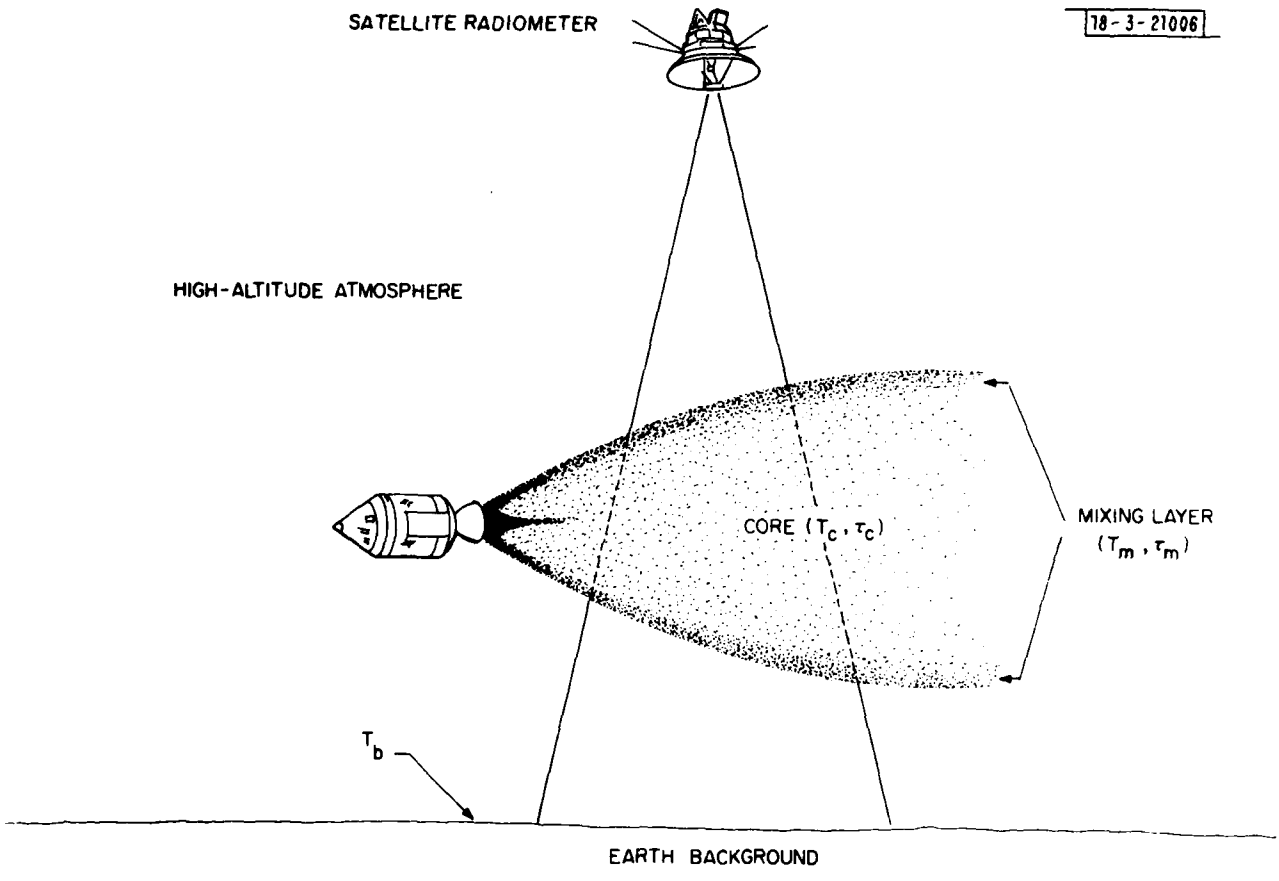

Fig.1. Core and mixing layer regions of high altitude rocket plume radiometric signature.

stagnation values of specific enthalpies, h_1 and h_2, of the two fluids on opposite sides of the mixing layer. Therefore, making the approximation that the mean fluid velocity $\vec{V}$ is nearly constant across the width of the mixing layer at a given point downstream, and assuming that the flow is stationary in the coordinate system fixed in the vehicle, we obtain

$$h + \frac{1}{2} V^2 + \frac{1}{2} \frac{\rho_1 \rho_2}{\rho^2} V_{12}^{*2} = y_1 (h_1 + \frac{1}{2} V_1^2) + (1-y_1)(h_2 + \frac{1}{2} V_2^2) \qquad (3a)$$

where V_{12}^* is the local velocity difference within the mixing layer, where the local fraction of atmospheric species has the value $y_1 = \rho_1/\rho$, and $\rho = \rho_1+\rho_2$ is the total mass density. Note that

$$y_1 \frac{1}{2} V_1^2 + (1-y_1) \frac{1}{2} V_2^2 = \frac{1}{2} V^2 + y_1(1-y_1) \frac{1}{2} V_{12}^2, \qquad (3b)$$

where $V_{12} = |\vec{V}_1 - \vec{V}_2|$. Subscript 1 refers to the atmosphere and 2 refers to the plume.

The mixture temperature T is a maximum T_m within the mixing layer when the local relative velocity V_{12}^* is zero and when the mass fraction of entrained air y_1 is given by

$$y_1 = \frac{1}{2} + \frac{h_1 - h_2}{V_{12}^2} \simeq \frac{1}{2} \qquad (4)$$

The approximation of constant specific heats may be used downstream, so that $h \simeq c_p T$, $h_1 \simeq c_{p1} T_1$, and $h_2 \simeq c_{p2} T_2$. Therefore, the temperature maximum is approximately

$$T_m \simeq \frac{c_{p1} T_1 + c_{p2} T_2}{c_{p1} + c_{p2}} + \frac{\frac{1}{4} V_{12}^2}{c_{p1} + c_{p2}} \quad . \tag{5}$$

For the following parameter values,

V_{12} = 5 km/s

$R_H = k/m_H = 0.83 \times 10^8$ erg/K-g

$c_{p1} = 0.14\ R_H$ (64% O_2, 36% N_2 by volume)

$c_{p2} = 0.19\ R_H$ (30% H_2, 30% CO or N_2, 10% CO_2, 30% H_2O by volume)

T_1 = 1000 K

T_2 = 100 K

for which

$$c_p = y_1\ c_{p1} + (1-y_1)\ c_{p2} = 0.165\ R_H$$

we obtain T_m = 2750 K, of which only 480 K arises from the first term of Eq. (5).

The ratio of water vapor optical depths for the mixing layer and the core for a given radiative transition is approximately given by

$$\frac{\tau_m}{\tau_c} \simeq \frac{n_m \ell_m}{n_c r} \frac{T_{c,x}}{T_{m,x}} \left(\frac{T_{c,r}}{T_{m,r}}\right)^{3/2} \left(\frac{T_{c,t}}{T_{m,t}}\right)^{1/2} M_c e^{-\frac{E}{k}\left(\frac{1}{T_{m,r}} - \frac{1}{T_{c,r}}\right)}, \qquad (6)$$

where n_m and n_c are the water vapor concentrations (cm^{-3}) in the mixing layer and the core, and M_c is the local Mach number in the core at this distance r downstream. The temperatures with subscript x denote the excitation temperatures for the two levels that yield the fractional population in the lower of the two levels (separated by energy E); and with subscript t, the translation temperatures that determine the thermal speeds.

To obtain a rough estimate of the ratio of optical depths, we set all three core temperatures to 100 K and all three mixing layer temperatures to 1000 K. The Boltzmann factor in Eq. (6) is approximated by the value 2 for the 557- and 752-GHz lines, and the Mach number $M_c \simeq 4$. For a nozzle diameter d, the core H_2O density (in the absence of H_2O-air collisions) is approximately

$$n_o \simeq 10^{17}(d/r)^2 \ cm^{-3}. \qquad (7a)$$

The mixing-layer H_2O density is approximately

$$n_m = n_o - n_c = n_o(1-e^{-r/\ell_c}) \simeq \frac{n_o r}{\ell_c} \qquad \text{for } r/\ell_c < 1, \qquad (7b)$$

where $n_c = n_o e^{-r/\ell_c}$ is the H_2O core density in the presence of H_2O-air collisions. Beyond $r \simeq \ell_c$, n_c decreases exponentially so that the core is no longer important. The mean-free-path for H_2O-air collisions, $\ell_c = m_1/(\sigma' \rho_1) \simeq 1$ km at 250-km altitude with $\sigma' \simeq 10^{-15}$ cm^2 as the H_2O-air collision cross-section.

We then obtain from Eq. (6) the ratio of optical depths

$$\frac{\tau_m}{\tau_c} \simeq 4 \times 10^{-3} \qquad \text{for } r/\ell_c < 1. \tag{8}$$

Assuming that we are calculating the ratio of antenna temperatures for the mixing layer and core sufficiently downstream that the core is just thin, then

$$\frac{\Delta T_m}{-\Delta T_c} \simeq \frac{(T_m - T)}{-(T_c - T)} \frac{\tau_m}{\tau_c} \simeq 0.04 \qquad \text{for } r/\ell_c < 1, \tag{9}$$

where T is the earth background temperature. Thus, we conclude that, though the mixing layer is hot, it is too thin to affect the signal due to the core, even if there were no Doppler shift between the two regions.

B. Plume Signature Calculations

A computer program (Plume 1) has been developed for the MIT Lincoln Lab IBM/370 machine to predict the intensities of the rotational lines of plume molecules such as water vapor or carbon monoxide at various distances from the rocket nozzle.

For the present, simplifying assumptions limit the results of the calculations to the high-altitude case (above 150 km), where no shock phenomena are expected to occur downstream because the interaction between plume gas and ambient air is too diffuse. The air mean-free-path for momentum-changing collisions is at least 100 meters long at these altitudes.

For water vapor, the radiative transport is calculated for all electric-dipole transitions, however weak, between pairs of rotational energy levels up to angular momentum quantum number J_m=10. A value of J_m=10 has been found to be just large enough to represent the bulk of the distribution of populations among the rotational levels for translational temperatures less than 1000 K that are encountered downstream. There are 605 electric-dipole radiative transitions for J_m=10. In general, the number of transitions N_s for an asymmetric rotor (*e.g.*, H_2O) is given by $N_s=(1/2)J_mN^2$, where $N=(J_m+1)^2$ is the number of energy levels. This cubic and quadratic dependence on J_m contrasts with the much simpler case of the linear (diatomic) molecule, carbon monoxide, for which $N=J_m+1$ and $N_s=J_m$, where both numbers rise only linearly with J_m.

The line intensities are calculated at present under the simplifying assumption of the "local approximation." This approximation is most useful where supersonic flow is present because a photon is emitted at a point in the flow with a resonant frequency that lies within a narrow range about the Doppler shift derived from the component of the mean flow velocity along the photon propagation direction.

After the photon propagates over a short distance, its frequency will no longer be resonant in this transition with the molecules at this new location

because they are moving with a different velocity component that is outside the narrow range required for resonance. The narrow frequency width is the result of small thermal (or micro-turbulent) velocities.

The flow is approximatly radially-directed from a point-like source at the center of the nozzle orifice. Generally, the vehicle velocity is not aligned axially, i.e., not collinearly with the central exhaust streamline. The streamlines are then pushed sideways by the broadside momentum transfer between air and plume streams. Figure 2 shows the plume core and mixing layer regions of the rocket exhaust for such a misaligned case.

The following sections describe, in general terms, how the thermodynamic, radiative and collisional properties were incorporated into the program.

1. *Thermodynamic Properties*

To demonstrate the capabilities of the program, the altitude range of 200 to 250 km was chosen for most of the calculations. This corresponds to an average air density of about 4×10^{9} particles-cm^{-3}, and a pressure of 4×10^{-10} atms.

The density and temperature of plume gas emerging from the nozzle were selected as 10^{17} cm^{-3} and 1000 K, respectively, and are representative of most engines. The gas density was taken to vary downstream as $(1+R^{2})^{-1}$, where R is the ratio of radial distance downstream to the characteristic distance over which the density falls to half the exit value. On the central axis this distance is slightly larger than the nozzle diameter in the Brook model(3). Details of the flow and the transverse dependence of properties through the mixing layer will be described in another report.

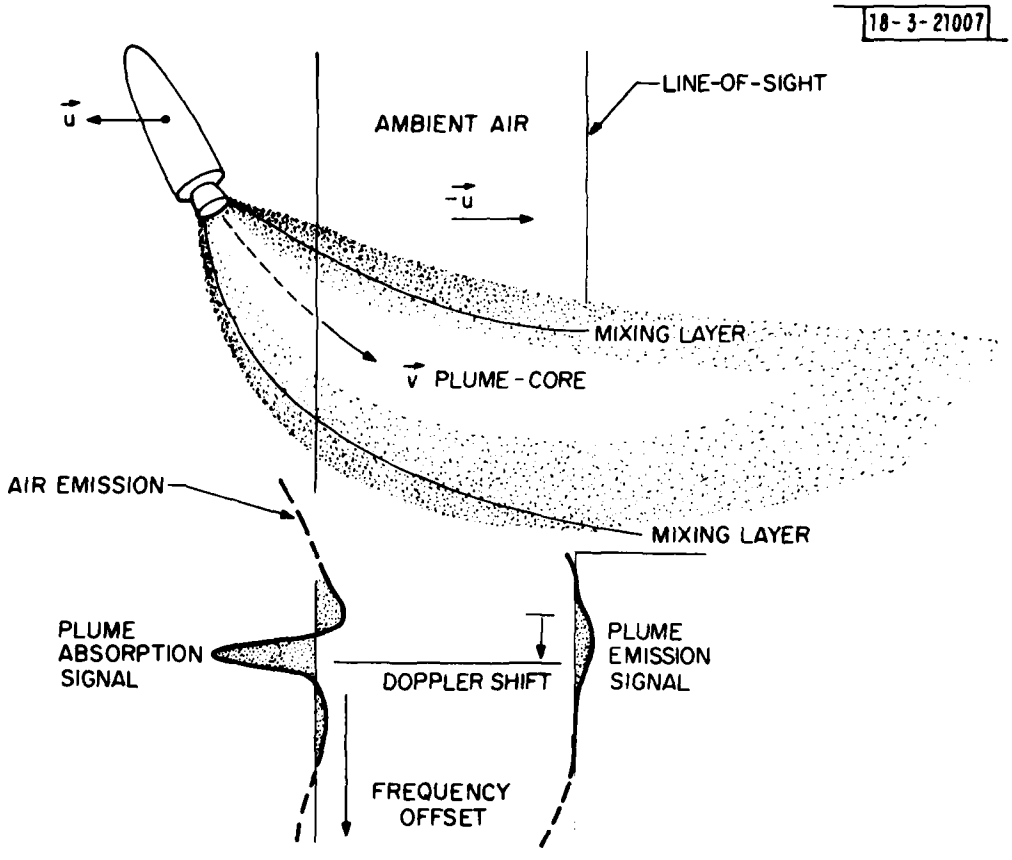

Fig.2. Model of plume core and mixing layer radiometric signals for high altitude plumes as a function of frequency for arbitrary line of sight.

The translational temperature of the plume gas is obtained from the energy equation that sets the rate of energy transfer from the air and from the internal degrees-of-freedom of the plume gas to the translational degrees-of-freedom of the plume gas equal to the sum of the rate of increase of the translational thermal energy and the rate of work done by volume expansion. To compute the translational temperature, the rate coefficients for transfer of translational energy from atmosphere to plume gases should range between 1 and 10 s^{-1} for the 200 to 250-km altitude range.

2. Radiative Properties

The line intensity and line shape of any transition is calculated as an excess radiation over the background continuum radiation corresponding to the temperature of 2.7 K of the cold sky or 250 K of the earth's atmosphere.

The intensity $\Delta I_{\mu\nu}$ of the excess radiation over the background is an integral, with respect to optical depth $\tau_{\mu\nu}$, of the product of $\exp(-\tau_{\mu\nu})$ and the difference between the source function S and the background intensity I_b. The optical depth $\tau_{\mu\nu}$ is the integral with respect to distance along a ray path (with direction cosine μ) of the absorption coefficient at frequency ν.

$$\Delta I_{\mu\nu} = \int d\tau_{\mu\nu}\, e^{-\tau_{\mu\nu}} (S-I_b). \tag{10}$$

In the local approximation, the optical depth is a quantity associated with each point in the flow and associated with the Doppler-shifted resonance frequency obtained from the component of the flow velocity along the ray direction.

The source function is the intensity given by the Planck function evaluated for the excitation temperature T_x, which is the effective Boltzmann temperature between the pair of levels whose transition is being considered. The excitation temperature is inversely proportional to the logarithm of the ratio of the two sublevel populations. Thus, the solution of the rate equations for the populations provides both T_x and $\tau_{\mu\nu}$ at each point in the flow for each transition.

When the local approximation is applied to the integral expression for the excess intensity, each point in the flow and each direction through that point has its assigned intensity obtained from the formula

$$\Delta I_{\mu\nu} = \frac{2h\nu}{\lambda^2}\left[\frac{1}{e^{h\nu/kT_x}-1} - \frac{1}{e^{h\nu/kT_b}-1}\right](1-e^{-\tau_{\mu\nu}}) , \qquad (11)$$

where T_b denotes the temperature of the background. In terms of antenna temperature T_A, the effective temperature difference between plume and background, Eq. (11) becomes

$$T_A = \Delta I_{\mu\nu}\, \lambda^2/2k \quad . \qquad (12)$$

The local approximation to the integral in Eq. (10) need not be used if the line shape is required to reflect accurately the Doppler effects of thermal and turbulent motions, as well as those of the mean flow. This approximation might still be retained by way of the photon escape probabilities to obtain

(from the approximate rate equations) the population densities that appear in the excitation temperatures and the optical depths which are to be used in the integral for the intensity.

3. Collisional Excitation Properties

The transition rate, due to thermal collisions, between any pair of energy levels separated by energy ΔE is given by the phenomenological formula for the de-excitation rate coefficient (s^{-1} per molecule)

$$C_i = C_i' (1 + a_i x) \exp(-b_i x), \tag{13}$$

where i labels the first of the colliding pair (e.g., H_2O - H_2O, O - H_2O, etc.) and $x = \Delta E/kT_i$. The temperature T_i is the translational temperature of the species colliding with H_2O, if H_2O is the radiating species being considered in the rate equation. If atomic oxygen of the ambient atmosphere is causing the excitation, then $T_i = T_0 = 1000$ K. In this case, the parameters $a_0 = 1$ and $b_0 = 2$ were chosen. For H_2O - H_2O collisions, $T_i = T$, the plume translational temperature at the point in question, and $a_{H_2O} = b_{H_2O} = 1$ were chosen. These values of the a and b parameters are selected based on previous experience with theoretical and experimental values known for the collision pairs H_2 - CO and HF - HF. It should be noted that if a_i is greater than b_i, the rate shows a maximum as a function of ΔE, which is a quantity that increases for two levels directly as the difference between their values of J, the total angular momentum quantum number. For the conditions under consideration, the value of C_i' for plume molecules is $10^{-11} cm^3\text{-}s^{-1}$, and for both

entrained air at temperature T and ambient air at T_0, the value of C_i' is 3×10^{-11} cm^3-s^{-1}. By comparison with this rate constant for rotational excitation, the rate constant for heating of the plume gas translational temperature by the air collisions at temperature T_0 is taken to be ten times larger.

High-speed collisions also occur because of the relative flow velocity that exists between the flow of plume gas and the ambient air. The inelastic collision rate coefficient for deexcitation of rotational levels in the plume gas, owing to this directed flux, is of the form

$$C = C'/F \quad s^{-1} \tag{14}$$

and the excitation rate coefficient is

$$C = C'(1-x_{cm})/F \qquad (x_{cm} < 1) \tag{15}$$

$$C = 0 \qquad (x_{cm} \geq 1),$$

where $x_{cm} = \Delta E/E_{cm}$ and E_{cm} is the energy available in the center-of-mass system of a collision, while F is a factor that makes the collisional excitation of H_2O levels with lower values of quantum number K_{-1} more probable. This trend was noted from quantal calculations made earlier for inelastic collisions of O and H_2O (internal Lincoln Laboratory memorandum). For these high-speed collisions, C' is chosen to be 10^{-9} cm^3 -s^{-1} (for 200-250 km altitudes and

a relative velocity of 5 km-s^{-1}). For the plume core (near the inner edge of the mixing layer), only 10% of the directed flux is assumed to be participating and the effective C' becomes 10^{-10} cm^3-s^{-1}.

4. Photon Escape Probabilities

The factor $\exp(-\tau_{\mu\nu})$ is the probability that a photon of frequency ν will travel a distance corresponding to the optical depth in the direction specified by the direction-cosine μ. When averaged over solid angle at a point and over frequency, as weighted with the local frequency distribution function $f(\nu-\nu_o)$ for thermal and microturbulent velocities, this factor becomes the photon escape probability β that multiplies the Einstein A- or B-coefficient in the appropriate rate equation. The probability modifies the radiation processes of spontaneous and stimulated emission and absorption for each transition. The frequency distribution function $f(\nu-\nu_o)$ is taken to be a Gaussian function centered on the resonant frequency ν_o that is Doppler-shifted by the parallel component of the mean flow velocity and Doppler-broadened by the root-mean-square random speed due to motion. The distribution function is normalized to have unity for its integral over frequency.

In the local approximation and the case of radial source flow with velocity proportional to the radius from the point source, the photon escape probability is given by

$$\beta = (1-e^{-\tau})/\tau, \tag{16}$$

where $\tau = \bar{\alpha}r/v$

and $$\bar{\alpha} = \frac{Ag_u}{8\pi}\left(\frac{n_\ell}{g_\ell} - \frac{n_u}{g_u}\right)\lambda^3 \quad s^{-1}$$

is the absorption coefficient after integration over frequency and after multiplying by wavelength λ to convert to Doppler-velocity units for frequency-offset from line center. The population densities and degeneracies in the lower and upper levels of the transition are denoted by n_ℓ and n_u, and g_ℓ and g_u respectively.

For the case of constant velocity in point-source flow, the photon escape probability becomes

$$\beta = \frac{2}{3\tau} - e^{-\frac{\tau}{2}}\left\{\frac{\tau}{3}\left[K_2\left(\frac{\tau}{2}\right) - K_1\left(\frac{\tau}{2}\right)\right] - K_1\left(\frac{\tau}{2}\right)\right\}. \tag{17}$$

This dependence of β on modified Bessel functions of the second kind can be shown to behave sufficiently like the exponential-type function of the previous case that the exponential version is used for the present, even though the constant velocity approximation is more realistic over the portion of plume of interest (i.e., where the temperature is low compared to the stagnation temperature).

The A-coefficient is determined from the relative line strength as calculated from the computer program TOP, provided by Harvard University Chemistry Department, for asymmetric rotors with centrifugal distortion. The rotational energies, however, are calculated from a program developed by Cook et al.(4) and provided by Prof. Frank Delucia of Duke University. This program corrects for centrifugal distortion more accurately so that the line frequencies are accurate to better than 1 MHz up to J=10.

5. Computational Method

The rate equation for the fractional population density n_i in the ith energy level has the form

$$v\frac{\partial n_i}{\partial r} = R_{in}(i,r) - R_{out}(i,r), \tag{18}$$

where R_{out}, the rate of departure from this level, is given by

$$R_{out}(i,r) = n_i \dot{\sigma}_i. \tag{19}$$

The coefficient $\dot{\sigma}_i$ is the sum of all rate coefficients, radiative and collisional, that carry population from the ith level to any other level. The flow velocity is v, which is a function of distance through the Bernoulli equation for diabatic conditions. The solution to the above equation, treated formally as linear, is

$$n_i(r) = n_i(r_o)e^{-\sigma_i(r_o,r)} + \int_{r_o}^{r} \frac{dr'}{v(r')} e^{-\sigma_i(r',r)} R_{in}(i,r'), \qquad (20)$$

where $\sigma_i(r',r) = \int_{r'}^{r} \frac{dr'}{v(r')} \dot{\sigma}_i(r')$. The exponential factors are the probabilities that population sources at upstream points r' of a streamline are felt downstream at the point r. For the present, straight radial streamlines may be imagined, but these are bent by interaction with the ambient air stream according to flow calculations to be described in another report.

The source term R_{in} is the sum of all sources from all levels denoted by the index j, that is,

$$R_{in}(i,r') = \Sigma_j n_j(r')\, W_{ji}(r'),$$

where
$$W_{ji} = A_{ji}(1+I_{ij})\,\beta_{ij} + C_{ji} \qquad (\text{if } E_j > E_i) \qquad (21)$$

$$= A_{ij}(g_i/g_j)\, I_{ji}\, \beta_{ji} + C_{ji} \qquad (\text{if } E_j < E_i),$$

depending upon whether E_j is greater or smaller than E_i, the energy of the ith level. An energy level diagram for the rotational levels of H_2O is shown in Fig. 3.

The non-dimensional intensity I_{ij} that appears above is the incident or background intensity associated with the earth's atmosphere (or the nozzle orifice) divided by $2h\nu/\lambda^2$. The collision coefficient C_{ij} (and C_{ji}) is the

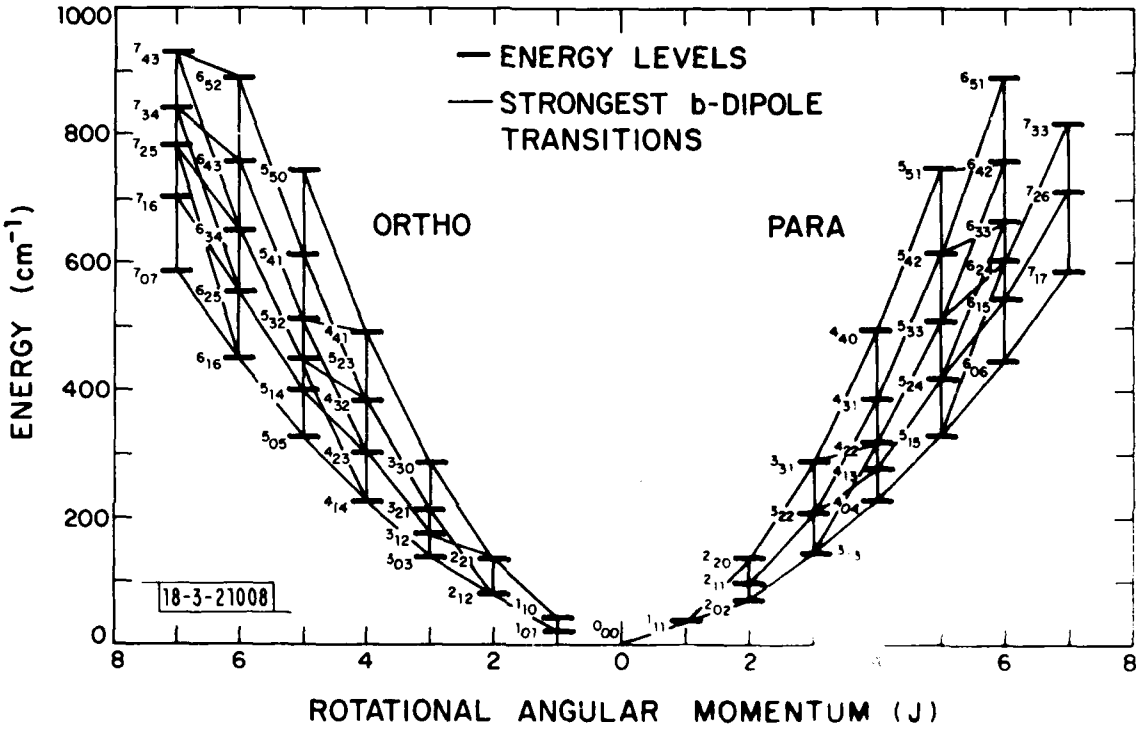

Fig.3. Water molecule rotational energy levels.

appropriate sum of the rate coefficients for all the different collision partners that induce transitions between levels i and j in the radiating species, e.g., H_2O.

The equations for the $n_i(r)$ are solved by iteration, i.e., by introducing the previously-obtained $n_j(r')$. The initial guesses are those of thermal equilibrium at the local translational temperature. For the present, all numerical integrations are done with the simple trapezoidal rule on a grid of points in the radial position variable R, the ratio of the position r to the characteristic length in the density law discussed earlier. The grid spacing is made wider for points farther downstream, where properties are found to vary more slowly.

6. Plume Signature

For the work reported here, the case of the streamlines of the plume core that lie near the inner edge of the mixing layer will be discussed. As shown in Fig. 4, the optical depth for the 557-GHz transition in water vapor may be substantial at distances downstream as great as 4000 nozzle diameters, for an altitude of 250 km, and 15,000 nozzle diameters for 350 km. Within this distance, the absorption of the background earth radiation would be significant if the plume were viewed from above. In Fig. 5, the excitation temperatures for the 557-GHz and 752-GHz transitions rise farther downstream (see Section 2), due to collisional heating by the ambient air stream, so that both the optical depths and differences between source function and background intensity are reduced. The diabatic temperature is the translational plume gas temperature taking into account heating by air-interaction and cooling by

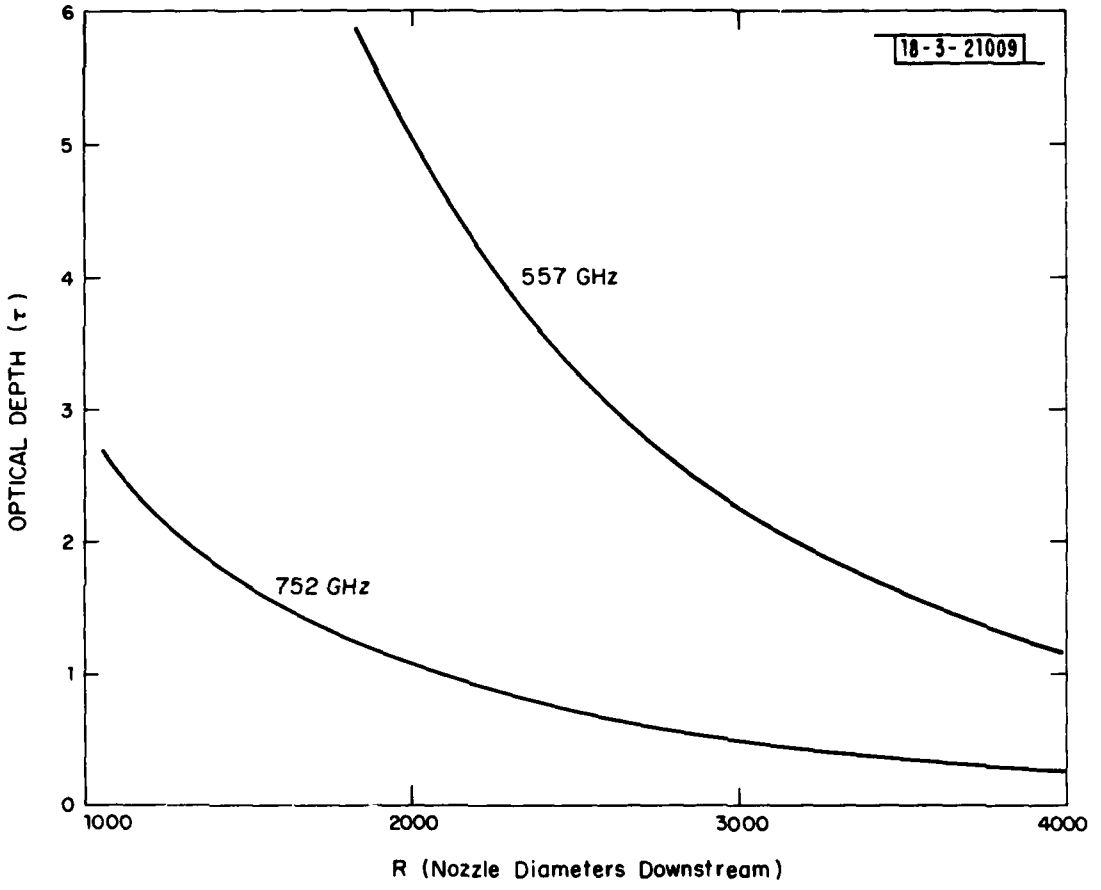

Fig.4. Optical depths at 250 km for 557- and 752-GHz water lines as a function of axial distance from the exhaust nozzle.

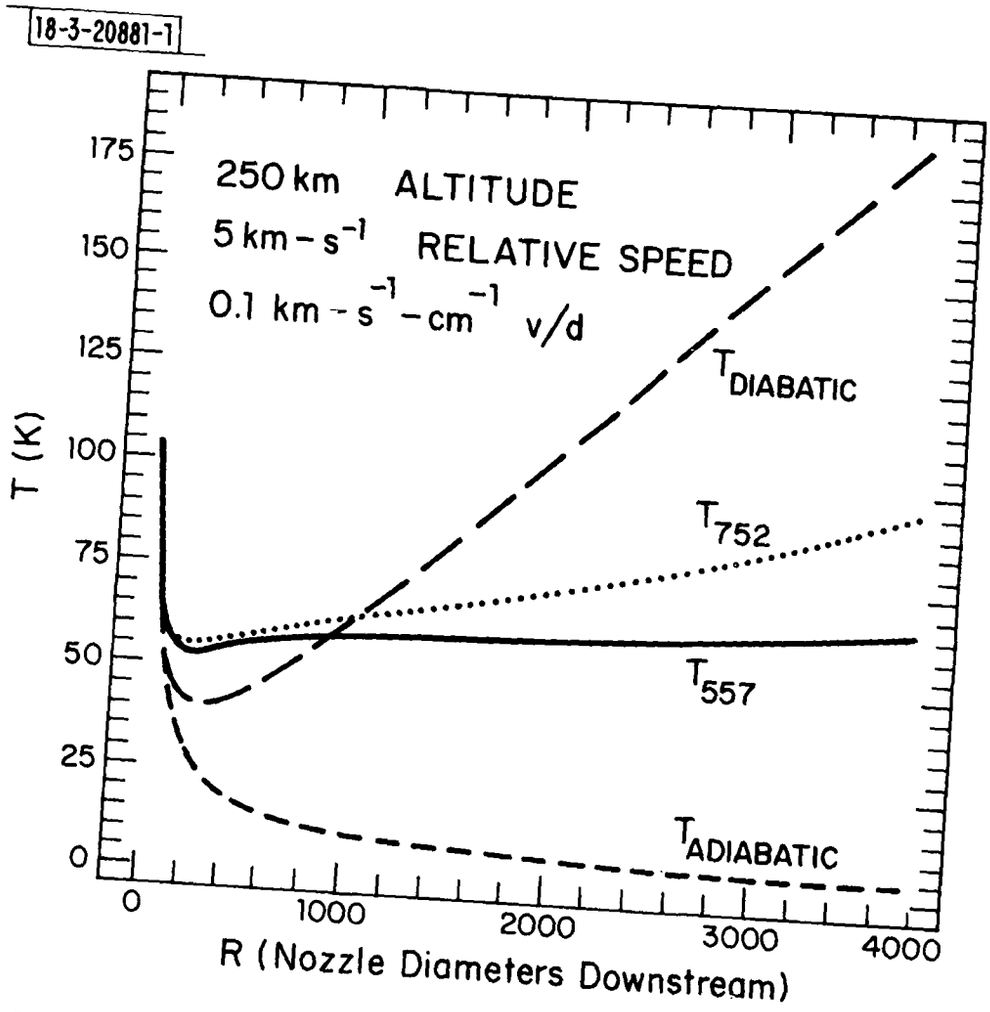

Fig.5. Plume temperatures at 250-km altitude as a function of axial distance from the exhaust nozzle.

volume expansion. The adiabatic temperature indicates this cooling effect when the air collisions are absent. The quantity v/d is the ratio of local exhaust velocity in the core (nearly constant with distance downstream) to the nozzle diameter. This quantity characterizes a typical flow rate (s^{-1}) to be compared with collisional and radiative rates.

Figure 6a shows the resulting behavior of the line intensities along a typical streamline (given in terms of antenna temperature T_A) for the emerging H_2O radiation at the 557- and 752-GHz frequencies. In Fig. 6b, the antenna temperatures of the 557-GHz line are compared at 250- and 350-km altitude, where it is seen how the plume signature can increase dramatically as the ambient air density falls off at even higher altitudes. In Fig. 7, an estimated typical 557-GHz plume signature is shown as a function of frequency offset (from rest frequency) against the absorption profile of the earth's atmosphere. The computer program is being extended to yield more accurate radiation intensities and profiles from detailed models of the mixing layers and core.

From these calculations, it may be concluded that rocket motors with thrusts of only a few thousand pounds at altitudes of 250 km may produce cold plume signatures large enough to provide sufficient beam fill for observation by submillimeter-wave heterodyne radiometers in synchronous orbit. At higher altitudes (e.g., above 350 km), motors with thrusts of a few hundred pounds may be detectable. Even with present far-infrared technology, observation of high-altitude plumes may be accomplished with antenna apertures of several meters in diameter and dwell times on the order of one second.

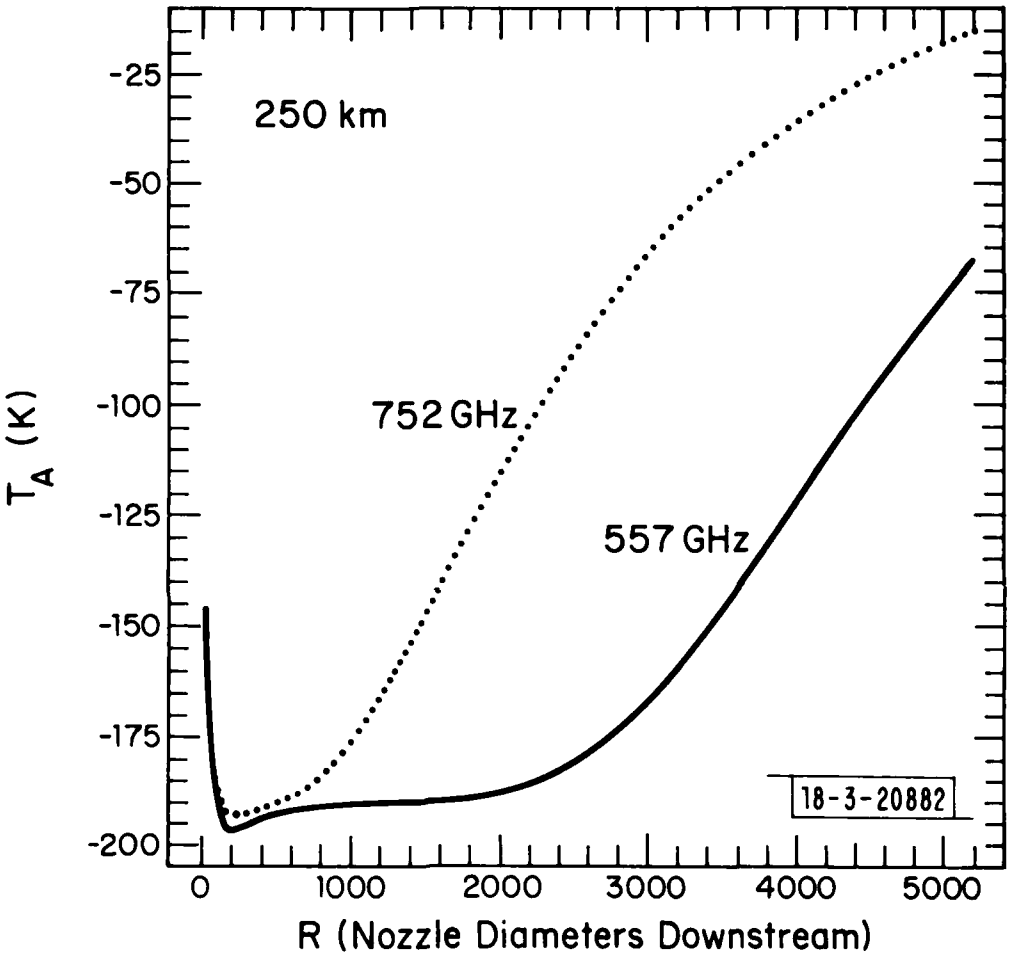

Fig.6a. Plume radiometric signals for 557- and 752-GHz at 250-km altitude against a 250-K earth background as a function of axial distance from the exhaust nozzle.

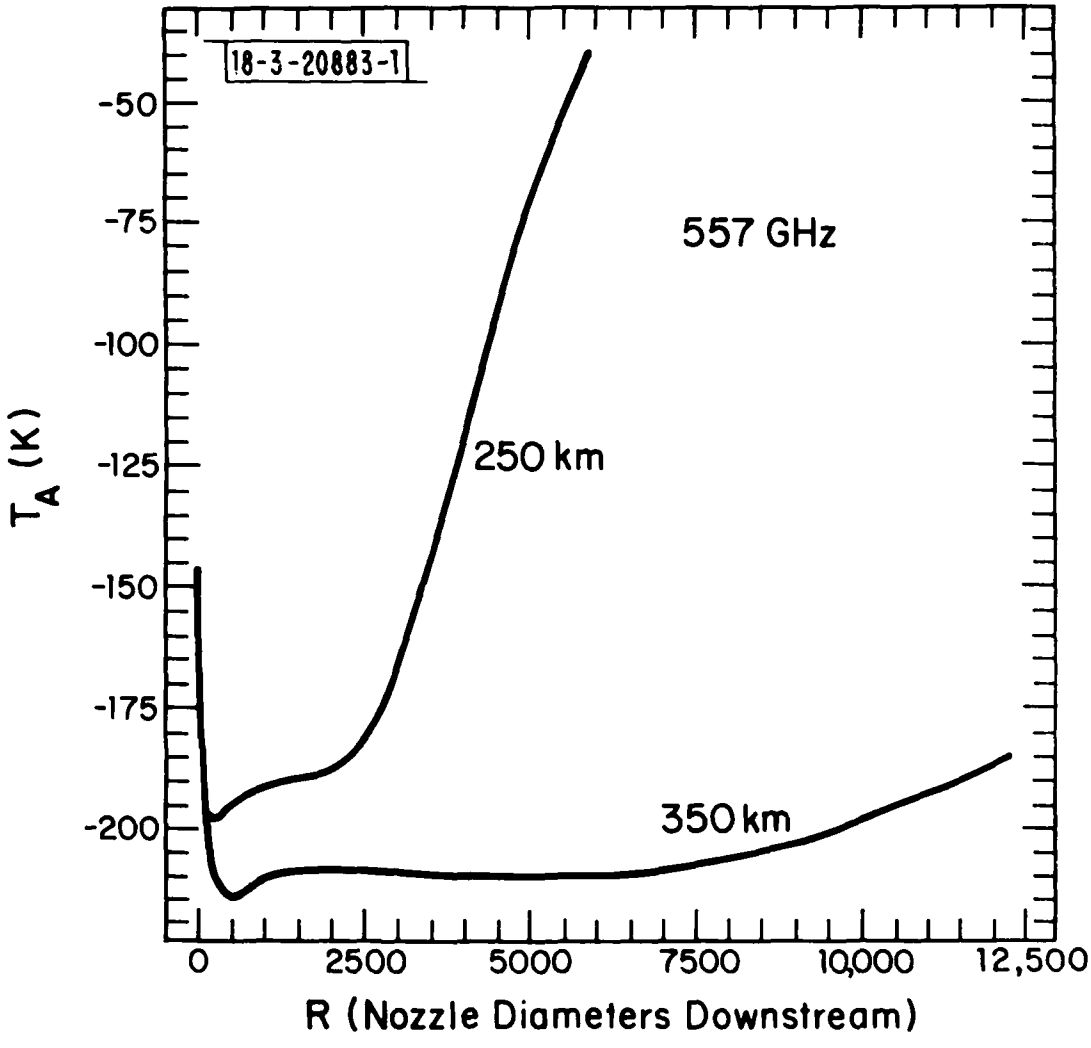

Fig.6b. Plume radiometric signals at 557 GHz against a 250-K earth background as a function of axial distance from the exhaust nozzle, at altitudes of 250 and 350 km.

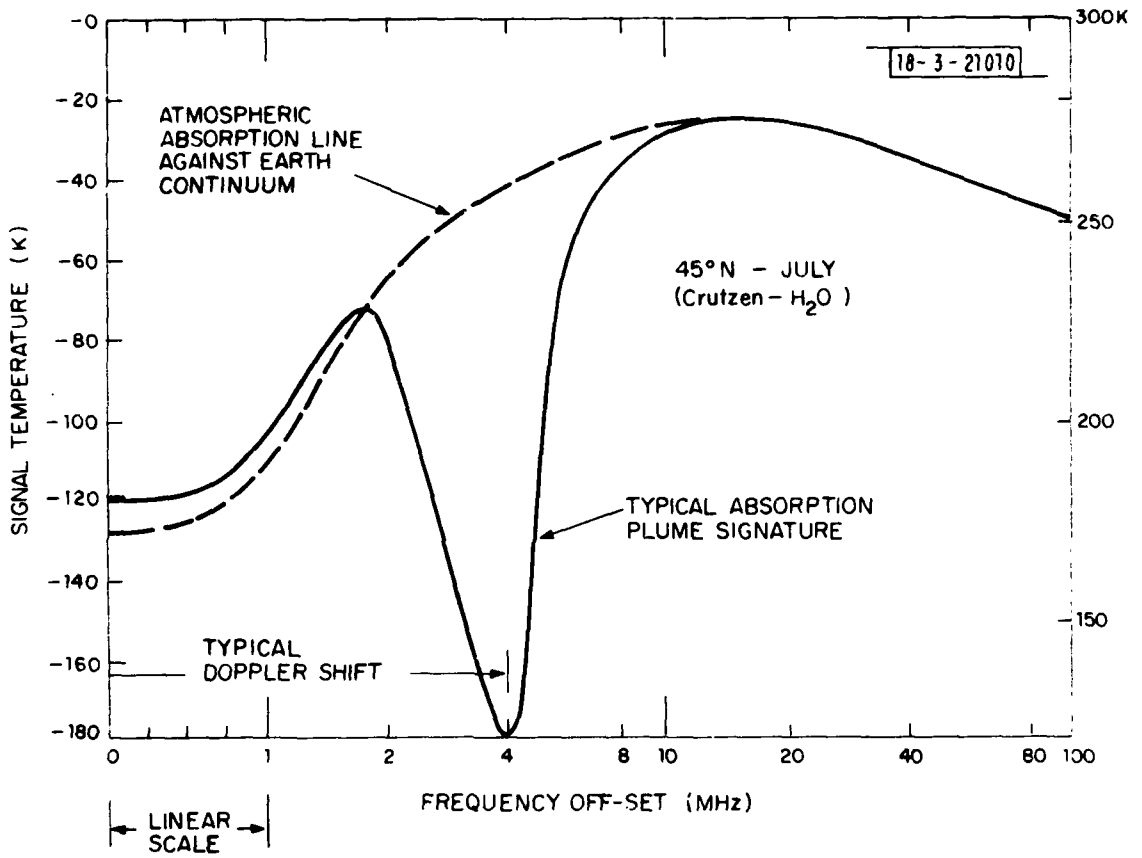

Fig.7. Atmospheric and plume water vapor 557-GHz signature.

III. EXPERIMENTAL TECHNIQUES

To examine experimentally the theoretical predictions of plume rotational temperatures and optical depths of submillimeter-wave absorption lines, two basic approaches are available for use with a laboratory-scale simulated plume. For surveying the entire spectral region of interest, a Fourier transform spectrometer is potentially the most appropriate instrument, and for studying the characteristics of selected absorption lines, a heterodyne receiver can provide the necessary capabilities. In both cases, sensitivity requirements for plume applications reach to current state-of-the-art limitations.

A. Simulated Water Vapor Plume

To diagnose the absorption (or emission) characteristics of an abiabatically expanding rocket plume with high water vapor content, a large high-vacuum chamber has been adapted to accommodate the operation of a laboratory-scale water vapor jet. Depicted in Fig. 8, the Lincoln Laboratory space environmental test chamber is approximately cylindrical with a diameter of three meters and a length of ten meters. Since the inner surfaces are almost entirely liquid-nitrogen cryopaneled, the chamber is ideally suited for pumping water vapor and is capable of reaching a background pressure of 3×10^{-7} Torr (simulating an altitude of 250 km). Since the vapor pressure of ice is virtually non-existent at 77 K, the jet effluent can continue to freeze on the chamber walls without an appreciable rise in pressure for

18-3-19610(1)

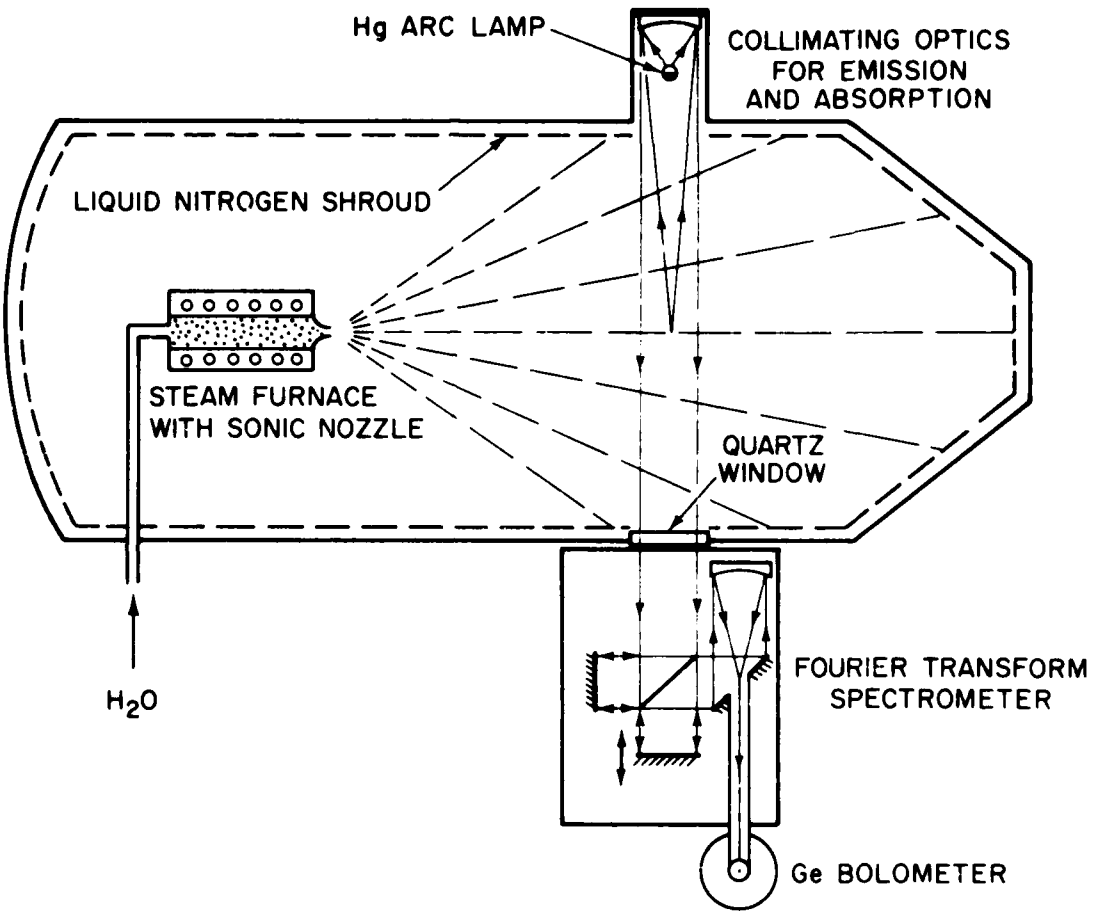

Fig. 8. Laboratory arrangement for spectral emission and absorption measurements at submillimeter wavelengths. Detection instrument can be a Fourier transform spectrometer (as shown) or a heterodyne radiometer.

several hours at mass flow rates on the order of 1 g/sec. In this manner, the high altitude conditions of a rocket plume core may be simulated with good accuracy.

Figure 9 is a sketch of the transparent gold furnace (5) used to generate the water vapor jet. Because of the absence of out-gassing, these furnaces are ideal for in-vacuum applications, where only an infrared radiation shield is required as insulation. A thin gold film evaporated onto the internal surface of the outer pyrex tube provides excellent reflective properties in the infrared, while rendering the furnace transparent at visible wavelengths. The inner reaction tube is made of quartz and is divided into two stages, with a baffle as a water dam. In the first stage, called the vaporization section, the water is brought to boiling. With the escaping steam passing over to the steam section, recommended stagnation conditions of 900 K temperature and 10 Torr pressure (6) may be achieved with modest amounts of heating power. The dimensions of the simulated plumes may be tailored according to nozzle diameters, and where necessary, by increasing the size and heating capacity of the gold furnace.

B. Fourier Transform Spectroscopy

As discussed in the Appendix, incoherent detection by means of a grating spectrometer is hampered by throughput limitations where high resolution is desired. A Fourier Transform Spectrometer (FTS) has the advantage of a throughput that is independent of resolution because the element width $\Delta\nu$ is determined by the maximum distance of mirror travel L (i.e., $\Delta\nu = 1/2L$). Since the instrument is essentially a Michelson interferometer (see Fig. 8) which continually

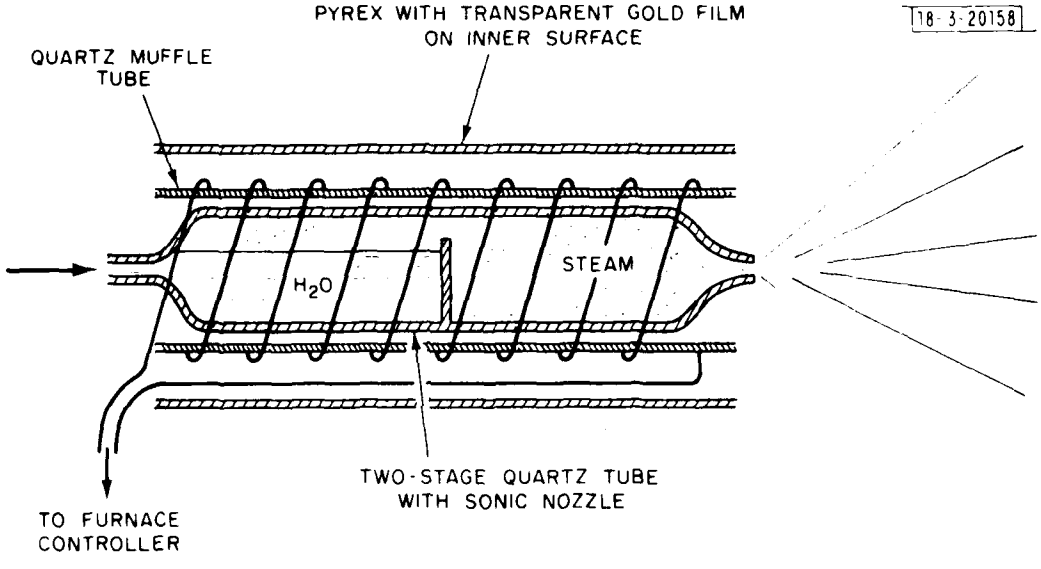

Fig.9. Laboratory-scale water vapor jet with sonic nozzle.

collects all of the spectral radiation from a given collimated source over a large predetection bandwidth (determined by the spectral band of the detector and any filters or windows in the optical path) as the moving mirror scans through a distance L, it is ideally suited for survey applications. This multiplexing advantage means that an FTS can scan with equivalent sensitivity the entire spectral region in the same time that a grating instrument would require to cover a single resolution element $\Delta\nu$.

For detector-noise limited operation in the Rayleigh-Jeans region (where $h\nu \ll kT_p, kT_b$), Eq. (A-4) and Eq. (A-9) for the ratio of signal to rms noise may be reduced to

$$\left(\frac{S}{N}\right)_{FTS} = \eta_1 \frac{2k\Delta T\nu^2\delta\nu \sqrt{t\eta_2(1-\eta_2)}A\Omega}{c^2(NEP)_{inc}} \tag{22}$$

where $\Delta T = (T_p - T_b)(1-e^{-\tau})$ and t is the total time of observation (or integration). Negative values of ΔT denote absorption and positive values denote emission. The optical depth τ of the plume appears in the exponential function. For this type of instrument, the collection efficiency η_1 is determined by the beamsplitter loss and any other losses associated with windows, filters and lightguides; the observation efficiency η_2 is fixed by the chopping cycle associated with synchronous detection and is normally equal to 1/2. For a step-and-integrate FTS, t represents the product of the sampling time (time for each step) and the total number of steps in one mirror scan. For the continuous-scan version, t is the time for one scan, multiplied by the number of

scans. Since mirror velocities are much greater in continuous scan models, there is usually time to carry out several scans in one experiment

With the particular instrument in use at Lincoln Laboratory for the spectroscopy measurements of an optically thick ($\tau > 1$) plume with $T_p = 50$ K, for example, the values of the experimental parameters are as follows:

$$\begin{aligned} T_b &= 3000 \text{ K} \quad \text{(Hg arc lamp)} \\ \delta\nu &= 10^{-5}\nu \quad \text{(Ref. 2)} \\ A\Omega &= 1.6 \text{ cm}^2\text{-ster} \\ (\text{NEP})_{inc} &= 5 \times 10^{-13} \text{ W-Hz}^{-1/2} \quad \text{(Ge bolometer)} \\ \eta_1 &< 0.25 \\ \eta_2 &< 0.5 \end{aligned} \tag{23}$$

Thus, Eq. (22) may be simplified to

$$\left(\frac{S}{N}\right)_{FTS} < 5 \times 10^{-7} \quad \nu^3\sqrt{t} \,, \tag{24}$$

with ν in GHz. For $\nu = 752$ GHz and a total integration time $t = 1$ s (achievable with a rapid-scan instrument)

$$\left(\frac{S}{N}\right)_{FTS} \leq 212 \tag{25}$$

for the 752-GHz water vapor absorption line ($2_{02} \rightarrow 2_{11}$, see Fig. 3). Similar results apply for the 557-GHz line ($1_{01} \rightarrow 1_{10}$).

The above estimate of the spectrometer sensitivity suggests that absorption measurements of plume lines may be carried out with little difficulty. However, this computation is based on the assumption that the system is limited to detector noise only and that the full multiplexing advantage of the FTS can be realized. The extent to which this assumption is valid depends on the intensity of other noise sources which may dominate the detector noise contribution. For a thorough description of the various noise sources, the reader is referred to the articles by Lowenstein (7) and Sakai (8), but the effects of two noise sources (photon and digitization) in the Lincoln Laboratory experiment are of immediate interest.

Where intense sources are combined with large optical throughputs, as in the case under discussion, the system may become background noise limited (photon or related noise from the high temperature mercury arc lamp). For example, with an incident total continuum power of 10^{-4} W, the lamp output stability must be better than 1 part in 10^{8} for one second durations, in order to insure that the noise is less than the Ge bolometer detector noise of 5×10^{-13} W.

Another serious noise contribution arises from the limited resolution capability of FTS instruments (see Fig. 10 showing a water vapor FTS spectrum taken over a 2-m path at 17 Torr). If the maximum resolution fraction $\delta\nu/\Delta\nu$ (the ratio of the spectral linewidth to the resolution element width) is less than 10^{-3}, the absorption signal will appear in the third figure of the digital

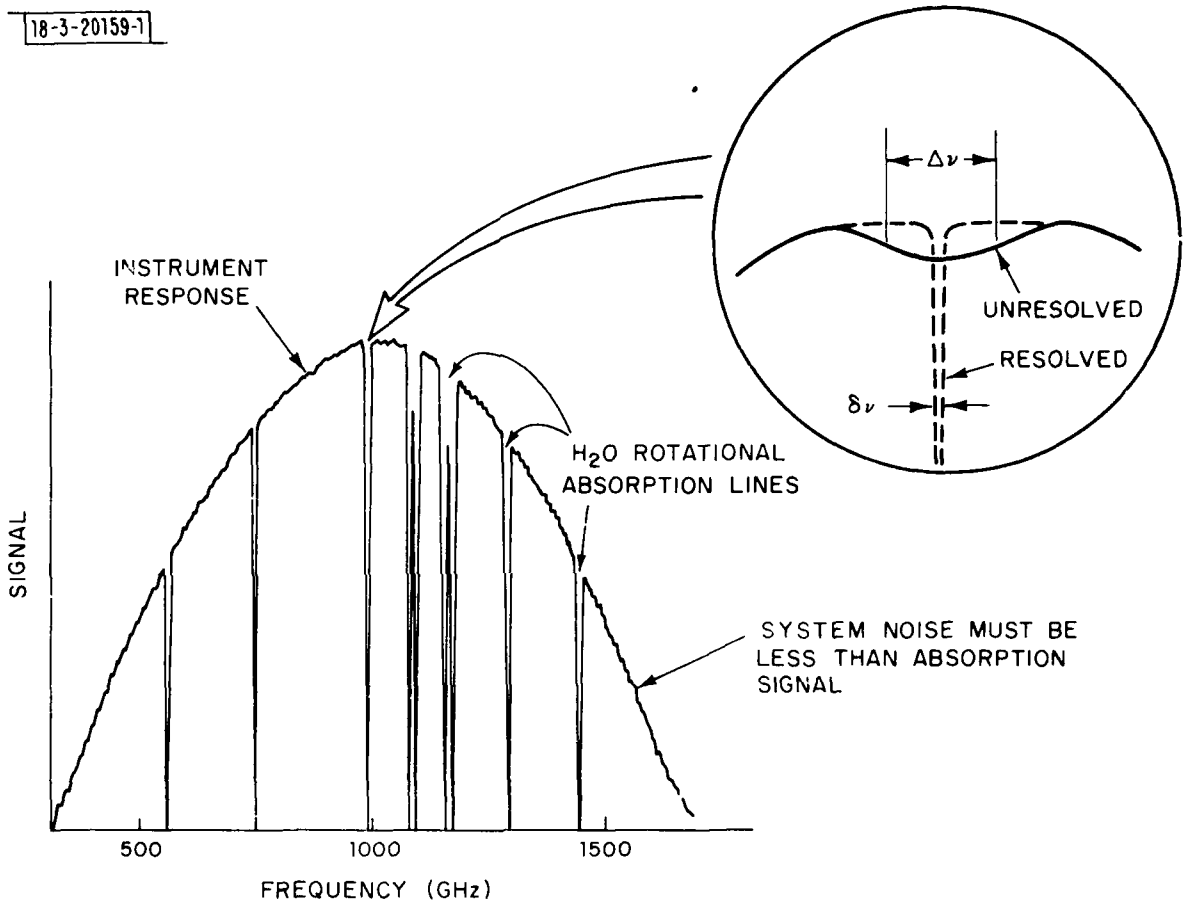

Fig.10. Typical Fourier transform spectrometer data for H_2O vapor at 17 Torr pressure over an optical path length of 2 m shows a completely resolved submillimeter-wave spectrum. When the spectral linewidth $\delta\nu$ is less than the resolution element width $\Delta\nu$, a loss in sensitivity occurs.

output. This means that the dynamic range of the analog-to-digital conversion system must be accurate to at least four figures, or fluctuations in the third digit will produce "digitization noise" that will contribute sufficiently that the multiplexing advantage will be lost and the sensitivity reduced accordingly.

As discussed in the Appendix, incoherent detection schemes are mainly suited to survey purposes, where high resolution is not a requirement. For studying radiative transfer in gaseous media, FTS is normally used only where collision broadening produces linewidths large enough to fall within the resolution capabilities of the instrument. Where Doppler broadening is dominant, unresolved absorption signals can be diminished by orders of magnitude, and the requirement for high dynamic range of analog-to-digital converters add further complications to the detection problem, because the absorption data may be contained only in the fourth or fifth digit. A spectrometer obtained commercially, such as the one available for the plume experiments, may require expensive modifications to increase the dynamic range. When a single spectral line is the object of investigation, a high-resolution heterodyne receiver is clearly a more suitable instrument, particularly at lower infrared frequencies.

C. Heterodyne Detection

The theoretical sensitivity of a heterodyne receiver operating in the Rayleigh-Jeans region (in one sense of polarization) may be deduced from Eq. (A-10):

$$\left(\frac{S}{N}\right)_{het} \simeq \eta_1 \frac{k\Delta T \ \mathrm{MIN}(\delta\nu, B_{if})}{(\mathrm{NEP})_{het}\sqrt{B_{if}/\eta_2(1-\eta_2)t} + N'} \qquad (26)$$

where η_1 is the antenna efficiency, including the beam-fill factor, and η_2 is again the observation efficiency. MIN($\delta\nu$, B_{if}) denotes the smaller of the two quantities: $\delta\nu$ and B_{if}. The above relation may be simplified further by assuming that the spectral linewidth $\delta\nu = B_{if}$, the IF (intermediate frequency) bandwidth. This condition will provide the maximum signal-to-noise ratio because there is no loss of signal per resolution width B_{if} from lack of resolution, which occurs when B_{if} increases beyond $\delta\nu$, and no further increase in noise per width B_{if} from the existing $\sqrt{B_{if}}$ dependence, which occurs when B_{if} decreases below $\delta\nu$. Although this latter case would provide more details of the line structure, it would do so only at the expense of reduced sensitivity (see Appendix).

In previous work (1), it was shown that $\delta\nu \simeq 10^{-5}\nu$ for Doppler-broadened spectral lines, and for single-polarization, single-sideband receivers, $(NEP)_{het} = h\nu/\eta_q$, where η_q is the quantum efficiency. With these substitutions for $\delta\nu$ and $(NEP)_{het}$, Eq. (26) may be written as

$$\left(\frac{S}{N}\right)_{het} = \eta_1 \eta_q \sqrt{\eta_2(1-\eta_2)}\; 2.1 \times 10^3\; \Delta T \sqrt{\frac{t}{\nu}}, \qquad (27)$$

where ν is given in GHz. For comparison with the FTS instrument, consider the following parameter values:

$$\nu = 752 \text{ GHz}$$

$$\Delta T = T_b - T_p = 3000 \text{ K} - 50 \text{ K} = 2950 \text{ K}$$

$t = 1$ sec.

$\eta_1 = 0.3$ (assuming 100% beam fill)

$\eta_q = 5.0 \times 10^{-3}$ (i.e., $(NEP)_{het} = 10^{-19}$ W/Hz)

$\eta_2 = 0.5$

Under these laboratory conditions, Eq. (27) yields

$$\left(\frac{S}{N}\right)_{het} = 169 \tag{28}$$

provided that the receiver is detector-noise limited. (For the satellite radiometer case, $T_b = 250$ K and $(S/N)_{het} = 14$.)

At submillimeter wavelengths, the heterodyne approach offers definite advantages over the FTS instrument, in the situation where only a single spectral line is to be investigated. In practice, the theoretical sensitivity of a coherent receiver is more easily realized because the resolution requirements are met by adjusting $B_{if} \simeq \delta\nu$. As a result, large dynamic ranges of readout instruments are not required and the problem of digitization noise is not encountered.

However, to construct a heterodyne receiver for operation at submillimeter wavelengths, there are two difficult technological requirements which must be met: 1) a mixer with low $(NEP)_{het}$ values, in this case about 10^{-19} W/Hz for 557-GHz water lines, and 2) a local oscillator (LO) capable of delivering milliwatts of power at frequencies close enough to the spectral line of interest for the use of microwave IF frequencies.

In Fig. 11, a sketch of a radiometric apparatus using a receiver of $(NEP)_{het} \simeq 10^{-19}$ W/Hz is shown for the measurement of a 77 K blackbody (immersed in liquid nitrogen)(9). The input signal is first chopped by a room temperature blade and then merged with a local oscillator (LO) signal from a submillimeter-wave laser through a diplexer. By means of an ellipsoidal or paraboloidal mirror, the input and LO signals are focused onto a Schottky-diode mixer mounted in a quasi-optical antenna fixture referred to as a corner-cube reflector (9). The details of the diode and reflector structure are shown in Fig. 12 with its antenna pattern data. Local oscillator power can be obtained from the submillimeter-wave laser sketched in Fig. 13, where a 40-W CO_2 laser delivering a 10.6-μm wavelength beam is used to furnish optical pumping of a far-infrared (FIR) laser, an end-mirrored cell which contains gas at a pressure on the order of 200 mTorr. To observe absorption by any water-vapor rotational line, this gas must be selected to provide FIR laser output at a neighboring frequency. For the 557-GHz line, difluoroethane ($C_2H_2F_2$) will produce power at 563 GHz; for the 752-GHz line, formic acid (HCOOH) will deliver a strong output (30 mW) at 761 GHz.

An attractive alternative to the submillimeter-wave laser LO is to use a harmonic frequency of a carcinotron power tube. For example, a carcinotron producing 1 watt of output power at 280 GHz may be employed for second harmonic (560 GHz) generation of several milliwatts, more than adequate to serve as the LO for a 557-GHz receiver. Harmonic mixing is a powerful tool in millimeter and submillimeter-wave technology and may also be used effectively for converting the heterodyne receiver to a spectrometer.

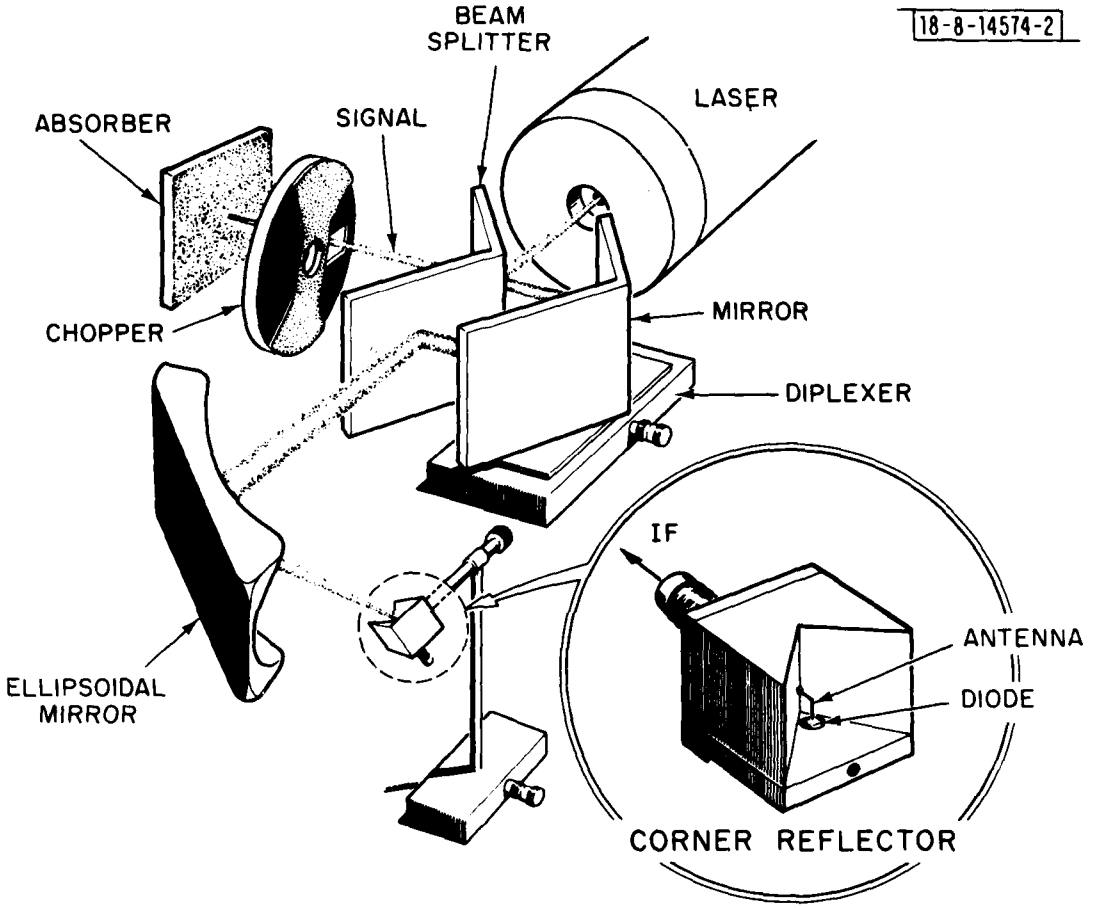

Fig.11. Heterodyne radiometer optics for blackbody temperature measurements (after Fetterman et al., Ref.9).

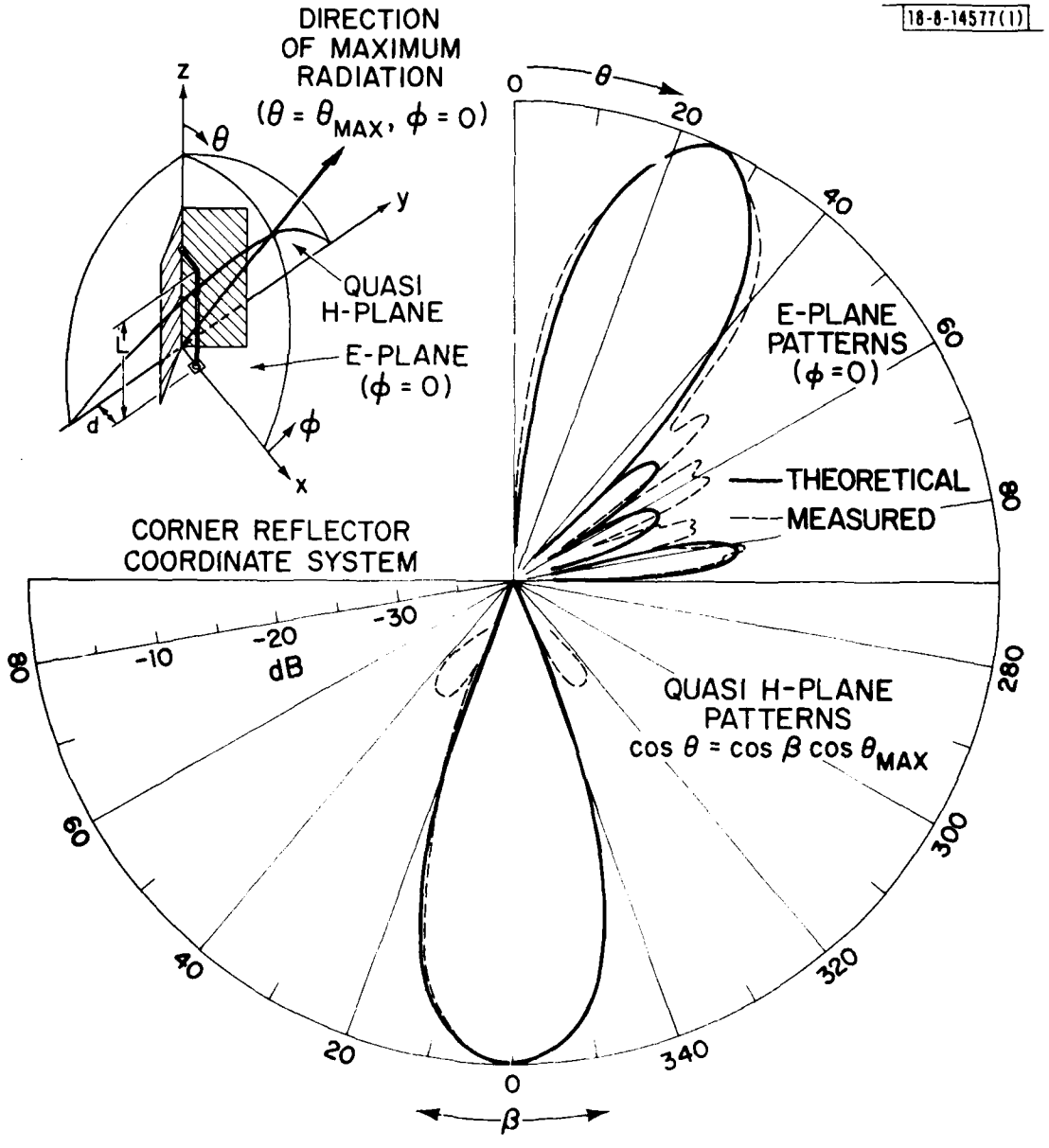

Fig.12. Corner-cube reflector antenna structure and pattern.

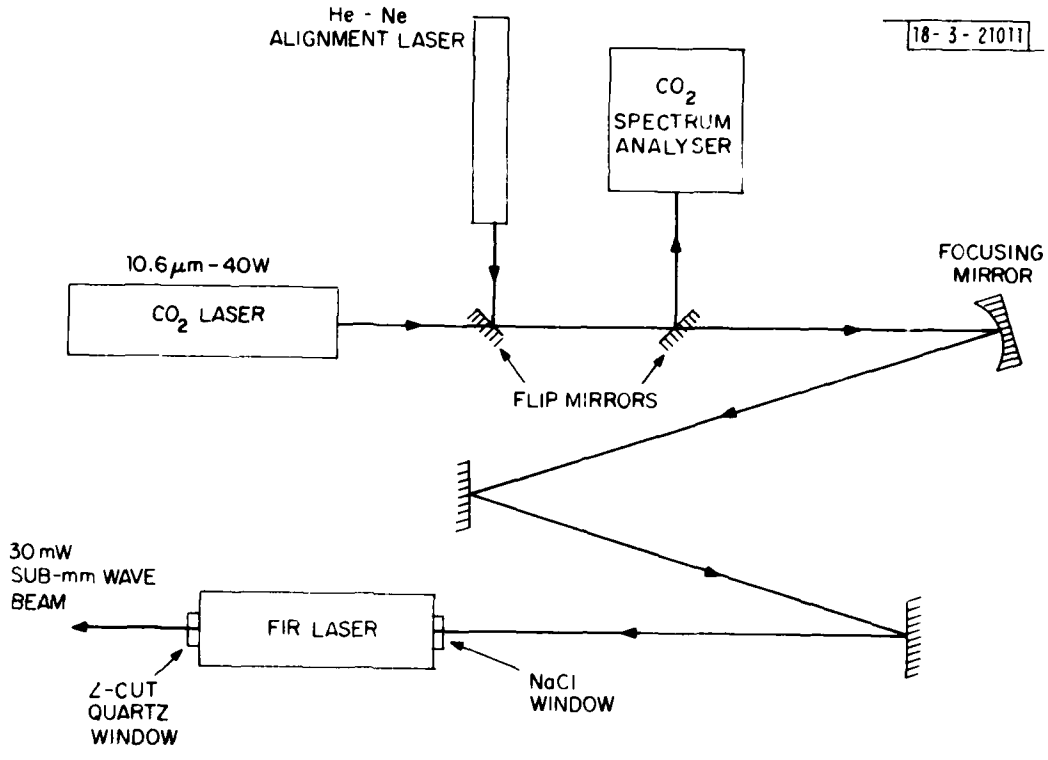

Fig.13. Optical arrangement for submillimeter-wave (FIR) laser with CO_2 laser pump source.

In Fig. 14, a second Schottky diode is employed to convert the heterodyne receiver into a spectrometer by first mixing the LO signal ν_{lo} with an independently generated IF signal ν_{if} to produce two sidebands at frequencies $\nu_{lo} + \nu_{if}$ and $\nu_{lo} - \nu_{if}$. In this manner, three submillimeter signals may be radiated through the plume, one of which is tuned to the desired water line frequency by adjusting ν_{if}. At the opposite port, the second mixer may be used to recover the IF signal from the two sidebands, and produce a very sensitive and highly selective (determined by the narrow bandwidth of the initial IF signal) measurement of the plume absorption. By sweeping the IF, a continuous display of the absorption line may be established (10).

Although this type of spectroscopic measurement will not by itself represent the basic radiometric situation described previously (1), it is a far more powerful technique for plume laboratory diagnosis, because it not only produces a more intense background signal (the effective temperature has been estimated at 10^{10} K), but also offers the capability of spatial mapping, since the off-axis paraboloid used to collimate the signal will produce a beam only a few centimeters in diameter at the center of the plume.

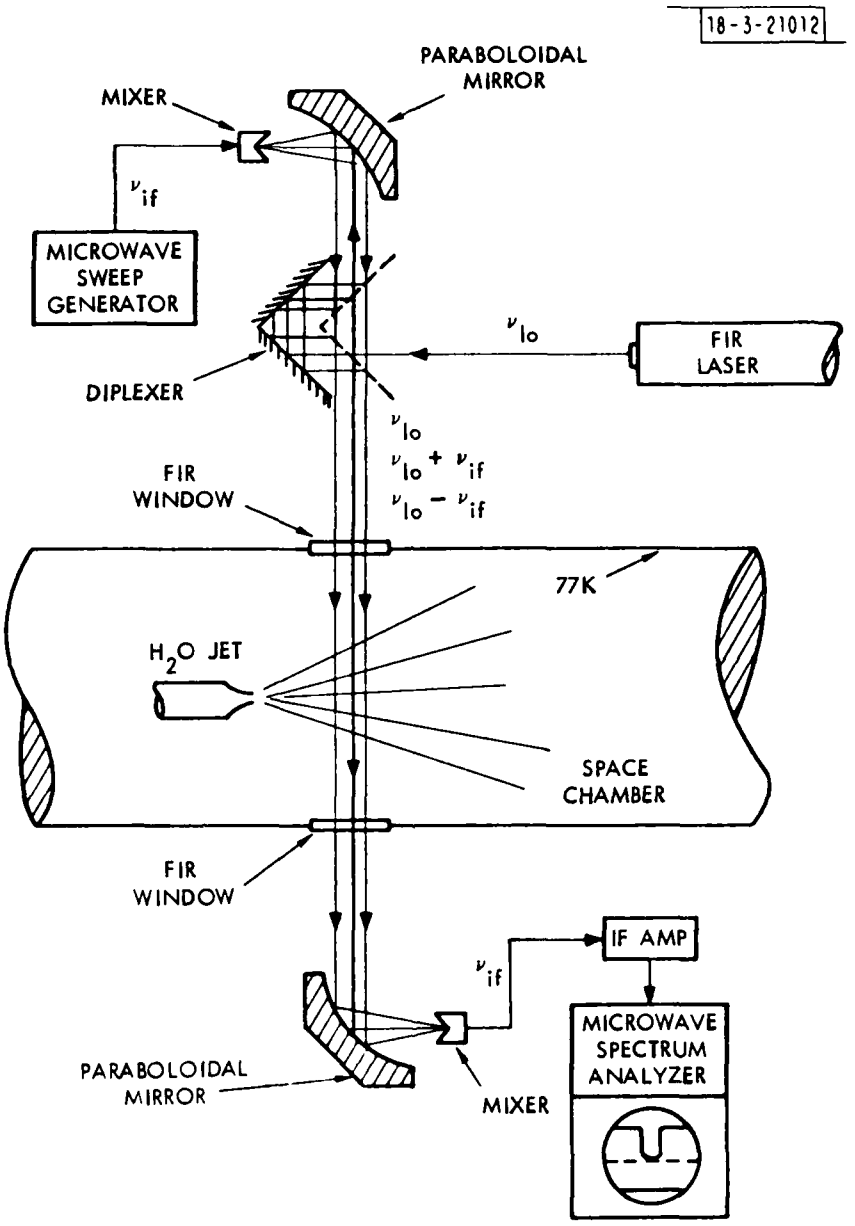

Fig.14. Submillimeter-wave spectrometer for high sensitivity, high frequency resolution measurements of plume water vapor absorption line.

IV. CONCLUSIONS

Based on the best theoretical estimates calculated from the PLUME 1 computer program, cold rocket plume core signatures thousands of nozzle diameters in length should exist for the 557-GHz and 752-GHz lines of water vapor. Signatures of this magnitude should make it possible for third stage and mid-course vernier motors at 250 km altitude, or bus motors at 350 km, to be observed with antenna apertures of several meters at dwell times of one second. Because of the transparency of the high temperature mixing layer which surrounds the cold core, the contribution from this region is not expected to have any significant impact on the effective temperature of the signature. For the case of the core optical depth on the order of unity, the mixing layer optical depth is about 20 times smaller.

With the recent development of a submillimeter-wave mixer capable of producing heterodyne receiver noise equivalent powers of 10^{-19} W/Hz, a radiometer for detecting cold plumes against a warm earth background is a technological reality. For a background temperature of 250 K, the cold core should be observable with a signal-to-noise ratio of 14 from synchronous orbit with post-detection integration times on the order of 1 second. Dwell times of only 10 ms should become possible when mixers with NEP values on the order of 10^{-20} W/Hz become available. Self-emission from the plume core is also detectable, but, for the same signal-to-noise ratio, only with dwell times that are longer by the square of the ratio $\Delta T/T_p$, where $\Delta T \simeq -200$ to -150 K when $T_p \simeq 50$ to 100 K, depending on plume altitude.

For laboratory-scale simulations, the requirements for beam fill are not difficult to meet because of the proximity of source to antenna. In addition, FIR lasers or carcinotrons with harmonic mixing, both cumbersome and inefficient LO power sources, may be used with relative convenience in a laboratory environment. A laboratory demonstration of the radiometric capabilities of the heterodyne receiver for observing cold rocket plumes at 557 and 752 GHz should be possible with these recent technological developments.

For field measurement, the extreme opacity of the lower atmosphere (troposphere) at 557 and 752 GHz renders unlikely the observation of rocket plumes from an aircraft at these frequencies. Only by means of a space platform, e.g., the Space Shuttle or high-altitude rocket probe, may a proper field measurement be carried out, and only at altitudes high enough to be capable of viewing the target against a 250-K earth background or against the cold sky. Therefore, field demonstrations of the feasibility of the submillimeter-wave cold plume detection concept will be dependent on: 1) the availability of a suitable space platform, and 2) the eventual development of an efficient, compact and preferably tunable source of local oscillator power. Although carcinotrons may be operated from a manned space laboratory, this latter requirement strongly suggests the need for improved solid-state technology in this area.

APPENDIX

A. Infrared Detector Concepts

For passive detection of a radiating source at temperature T, the brightness spectral distribution is given by the Planck formula

$$b(\nu,T) = \frac{2h\nu^3}{c^2}\left(\frac{1}{e^{h\nu/kT}-1}\right) \tag{A-1}$$

in units of $W\text{-}cm^{-2}\text{-}ster^{-1}\text{-}Hz^{-1}$, where h is Planck's constant, k is Boltzmann's constant, c is the speed of light, and ν is the frequency.

When a radiating plume source at excitation temperature T_p is detected against an equivalent blackbody continuum background of temperature T_b, the resultant brightness is

$$b_p(\nu,T_p) = b(\nu,T_p)(1-e^{-\tau_\nu}) \tag{A-2}$$

$$b_b(\nu,T_b) = b(\nu,T_b),$$

where τ_ν is the optical depth of the plume. The second factor, in parentheses, accounts for thin sources radiating less than the effective blackbody. The resultant brightness contrast may be represented by

$$\Delta b(\nu,T_p,T_b) = b_p(\nu,T_p)(1-e^{-\tau_\nu}) + b_b(\nu,T_b)e^{-\tau_\nu} - b_b(\nu,T_b)\ , \tag{A-3}$$

which reduces to

$$\Delta b(\nu,T_p,T_b) = [b_p(\nu,T_p) - b_b(\nu,T_b)](1-e^{-\tau_\nu}) \quad . \tag{A-4}$$

For a source of area A, which emits over a solid angle Ω that can reach the detector, the signal power over a bandwidth $\Delta\nu$ is given by

$$S = \Delta b \delta \nu A \Omega, \tag{A-5}$$

assuming 100% collection efficiency to the detector.

The product $A\Omega$ is commonly referred to as the "throughput" or "etendue" of an optical system and is an important factor in determining the radiation gathering capability of a receiver. For incoherent detection systems, $A\Omega$ is independent of frequency and is limited only by the geometrical factors associated with the practical size of the source and receiver aperture (see Fig. 15). With coherent or heterodyne systems, the received signal is that contained within the main antenna beam of solid angle Ω, corresponding to an effective antenna area A, and the throughput

$$A\Omega = \lambda^2 = \frac{c^2}{\nu^2} \quad , \tag{A-6}$$

according to the conditions of diffraction (11).

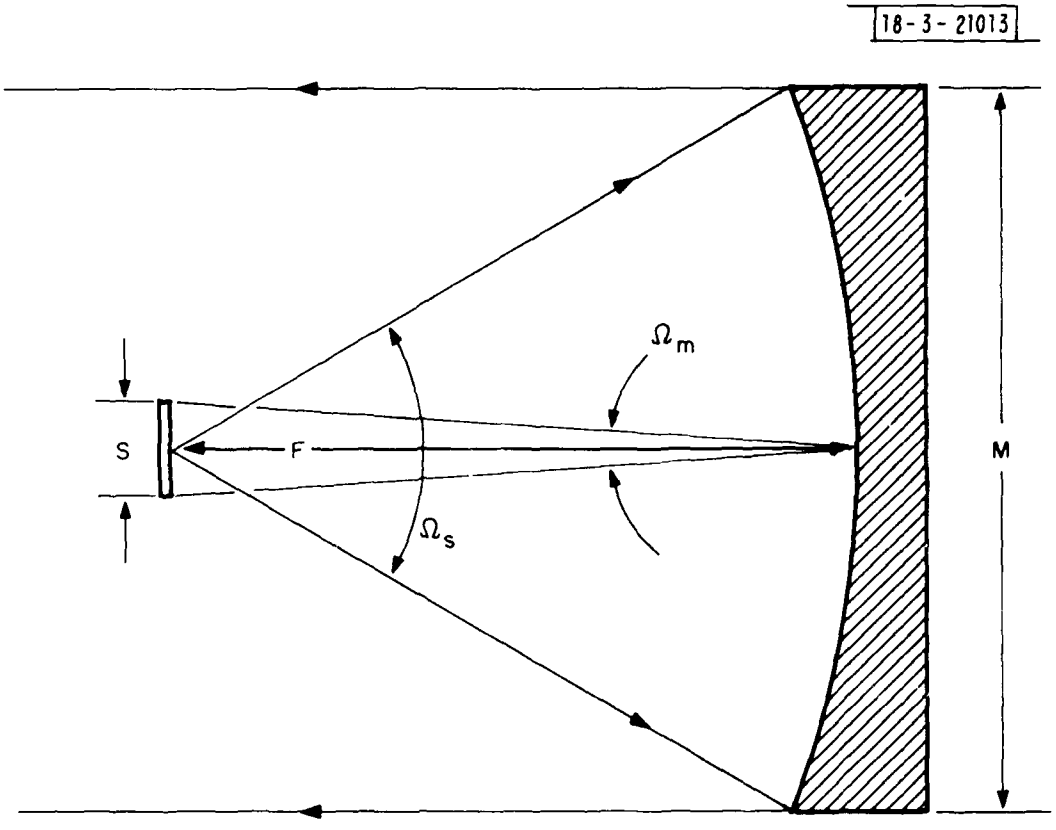

Fig.15. Geometrical optics definition of "throughput" $A\Omega$. Quantities with subscript m refer to the collecting mirror, whose effective aperture diameter is M and focal length is F, while quantities with subscript s refer to the source (arc lamp, e.g.) of effective diameter S. Note that the throughput for the source equals that for the mirror:

$$A_s\Omega_s = A_m\Omega_m = \frac{\pi S^2}{4}\,\frac{1}{F^2}\,\frac{\pi M^2}{4} \quad .$$

In general, the rms noise of an incoherent system may be expressed as

$$N_{inc} = (NEP)_{inc}/\sqrt{t} + N' \tag{A-7}$$

where $(NEP)_{inc}$ is the noise-equivalent power in W-Hz$^{-1/2}$ of the detector, t is the postdetection integration time, and N' is the power contribution from non-random noise sources.

The corresponding relation for the rms noise of a heterodyne receiver is

$$N_{het} = (NEP)_{het}\sqrt{B_{if}} / \sqrt{t} + N', \tag{A-8}$$

where B_{if} is the IF bandwidth and $(NEP)_{het}$ is the noise equivalent power in units of W-Hz^{-1}.

After combining Eqs. (A-5) through (A-8) and introducing efficiency factors, sensitivity relations may be written as

$$\left(\frac{S}{N}\right)_{inc} = \eta_1 \frac{\Delta b \delta\nu \, A\Omega}{(NEP)_{inc}/\sqrt{t\eta_2(1-\eta_2)} + N'} \tag{A-9}$$

and

$$\left(\frac{S}{N}\right)_{het} = \eta_1 \frac{\Delta b \delta\nu \, (c^2/\nu^2)}{(NEP)_{het}\sqrt{B_{if}}/t\eta_2(1-\eta_2) + N'} , \tag{A-10}$$

when B_{if} exceeds $\delta\nu$. When $B_{if} < \delta\nu$, the spectral linewidth, the total signal in the channel of width B_{if} is reduced by the fraction $B_{if}/\delta\nu$ and represents the condition of resolving the spectral line. When $B_{if} > \delta\nu$, the line is unresolved and the noise in the channel of width B_{if} is larger than it need be. Obviously, the optimum signal-to-noise ratio occurs when $B_{if} \simeq \delta\nu$. The efficiency η_1 is for the antenna, including the beamfill factor, and η_2 is the fraction of the observation or integration time t that is devoted to the plume, as opposed to the comparison or reference source during the remaining time.

B. Coherent Versus Incoherent Detection

For infrared detection, the relative merits of coherent and incoherent systems depend to a large extent on the frequency range and degree of frequency resolution involved in the particular application. Basically, there are three areas where these schemes differ, 1) the collected signal, 2) the detector noise, and 3) the resolution capability.

As described earlier, the amount of detectable signal power is determined by the throughput $A\Omega$ in either case. For the incoherent system, $A\Omega$ is independent of wavelength and is limited only by the geometrical factors associated with the collection optics or antennae. With diffraction-limited heterodyne receivers, $A\Omega = \lambda^2$, as determined by the main beam of the antenna, with the result that the signal received is usually much less than that of an incoherent system, when considering shorter wavelengths. Only in the millimeter-wave or far-infrared regions will the coherent detector become competitive if spectral resolution is not a consideration. However, because the ultimate NEP of a

heterodyne receiver is approximately the energy of a single photon $h\nu$, i.e., the "quantum limit" (12), the minimum detectable signal power is usually much smaller than that of an incoherent system, particularly where the predetection bandwidth B_{if} is small. This feature of heterodyne detection offsets its lower signal-collecting capability to some extent and further enhances its sensitivity at lower frequencies.

Finally, for high frequency-resolution applications, heterodyne receivers have a considerable advantage over incoherent systems. For diffraction grating and Fourier transform spectrometers, the minimum resolution cell $\Delta\nu$ is on the order of a few GHz, while the resolution limit of a heterodyne receiver is determined by the values of B_{if}, which may be less than a MHz. Because $\Delta\nu$ for a grating instrument is determined by the aperture slit width, the magnitude of A is proportional to $\Delta\nu$ and it may be argued from Eq. (A-9) with $\Delta\nu = \delta\nu$, the linewidth,

$$\left(\frac{S}{N}\right)_{grat} \propto (\delta\nu)^2 , \tag{A-11}$$

while for an FTS the aperture is fixed, and

$$\left(\frac{S}{N}\right)_{FTS} \propto \delta\nu . \tag{A-12}$$

However, since $B_{if} = \delta\nu$ for maximum sensitivity of a heterodyne receiver, Eq. (A-10) indicates that

$$\left(\frac{S}{N}\right)_{het} \propto \sqrt{\delta\nu} \qquad \text{(A-13)}$$

Thus, the heterodyne detector is not only capable of higher resolution, but its sensitivity is less dependent on $\delta\nu$ and will not decrease as severely when high resolution is achieved.

ACKNOWLEDGMENT

The authors are indebted to Drs. H. R. Fetterman, W. A. Blumberg, and P. E. Tannenwald for general guidance in the instrumentation concepts associated with far infrared heterodyne receiver technology. Gratitude is also expressed to Dr. G. Sollner of the University of Massachusetts and Dr. T. S. Chang of Northern Essex Community College for assistance with the Fourier transform spectrometer theory.

REFERENCES

1. G. F. Dionne, J. A. Weiss, and M. M. Litvak, "Radiometer Requirements for High Altitude Rocket Plume Observation at Submillimeter Wavelengths", Technical Note 1978-3, Lincoln Laboratory, M.I.T. (31 January 1978, reissued 1 August 1978), DDC AD-B029247.

2. T. J. Rieger, K. S. Tait, and H. R. Baum, "Atmospheric Interaction Radiation from High Altitude Rocket Exhausts," J. Quant Spectrosc. Radiat. Transfer 13, 1117 (1975).

3. J. W. Brook, J. Spacecraft and Rockets, 6, 626 (1969).

4. R. L. Cook, F. C. DeLucia, and P. Helminger, J. Mol. Spectros. 41, 123 (1972).

5. "Solid State Research", Lincoln Laboratory, M.I.T. (1969:1), p. 21, DDC AD-690997.

6. E. A. Sutton, "Design Considerations for a Laboratory Jet Simulating Rocket Exhausts," Concord Sciences Corporation Report CSC RN-4 (1977).

7. E. V. Lowenstein, "Fourier Spectroscopy: An Introduction," Aspen Int. Conf. on Fourier Spectroscopy, (1970), p.3, DDC AS-724 100.

8. K. Sakai, "Consideration of the Signal-to-Noise Ratio Fourier Spectroscopy," Aspen Int. Conf. on Fourier Spectroscopy, (1970), p. 19, DDC AD-724 100.

9. H. R. Fetterman, P. E. Tannenwald, B. J. Clifton, C. D. Parker, W. D. Fitzgerald, and N. R. Erickson, "Far-IR Heterodyne Radiometric Measurements with Quasi-Optical Schottky Diode Mixers," Appl. Phys. Lett. 33, 151 (1978).

10. W. A. Blumberg, H. R. Fetterman, D. D. Peck, and P. F. Goldsmith, "Tunable Submillimeter Sources Applied to the Excited State Rotational Spectroscopy and Kinetics of CH_3F," submitted to Appl. Phys. Lett. and reported at 1979 Conf. on Laser Engineering and Applications (Washington, D. C.).

11. J. D. Kraus, Radio Astronomy, (McGraw-Hill, New York, 1966), p. 157.

12. F. R. Arams, Infrared-to-Millimeter Wavelength Detectors, (Artech House, Inc., Dedham, MA, 1973), p.17.

UNCLASSIFIED

SECURITY CLASSIFICATION OF THIS PAGE *(When Data Entered)*

REPORT DOCUMENTATION PAGE

READ INSTRUCTIONS BEFORE COMPLETING FORM

1. REPORT NUMBER: ESD-TR-79-264	2. GOVT ACCESSION NO.
3. RECIPIENT'S CATALOG NUMBER	
4. TITLE *(and Subtitle)*: Detectability of Cold Rocket Plumes	5. TYPE OF REPORT & PERIOD COVERED: Technical Note
	6. PERFORMING ORG. REPORT NUMBER: Technical Note 1979-48
7. AUTHOR(s): Gerald F. Dionne, Jerald A. Weiss, Marvin M. Litvak, William D. Fitzgerald	8. CONTRACT OR GRANT NUMBER(s): F19628-80-C-0002
9. PERFORMING ORGANIZATION NAME AND ADDRESS: Lincoln Laboratory, M.I.T., P.O. Box 73, Lexington, MA 02173	10. PROGRAM ELEMENT, PROJECT, TASK AREA & WORK UNIT NUMBERS: Project No. 8X363304D215
11. CONTROLLING OFFICE NAME AND ADDRESS: Ballistic Missile Defense Program Office, Department of the Army, 5001 Eisenhower Avenue, Alexandria, VA 22333	12. REPORT DATE: 11 October 1979
	13. NUMBER OF PAGES: 64
14. MONITORING AGENCY NAME & ADDRESS *(if different from Controlling Office)*: Electronic Systems Division, Hanscom AFB, Bedford, MA 01731	15. SECURITY CLASS. *(of this report)*: Unclassified
	15a. DECLASSIFICATION DOWNGRADING SCHEDULE

16. DISTRIBUTION STATEMENT *(of this Report)*

Approved for public release; distribution unlimited.

17. DISTRIBUTION STATEMENT *(of the abstract entered in Block 20, if different from Report)*

18. SUPPLEMENTARY NOTES

None

19. KEY WORDS *(Continue on reverse side if necessary and identify by block number)*

high altitude rocket plumes
plume signature
submillimeter-wave radiometers
heterodyne radiometer

20. ABSTRACT *(Continue on reverse side if necessary and identify by block number)*

The problem of detecting high altitude rocket plumes with satellite-borne submillimeter-wave radiometers is examined from both theoretical and experimental points of view. To estimate the sizes of plume signatures contrasted against a 250-K earth background or in self-emission against the cold sky, a computer program has been developed to predict plume brightness temperatures and optical depths of rotational lines of plume molecular constituents (e.g., H_2O) as a function of distance from the nozzle. The methods employed in the computations are described in general terms, and examples are presented to indicate that detectable H_2O signatures extending to several thousand nozzle diameters should exist at plume altitudes above 250 km. Details of a laboratory water vapor jet operating in a high vacuum environment designed to simulate a rocket plume at high altitude are outlined. Sensitivity considerations relevant to the plume detection problem are discussed for Fourier transform spectrometers and heterodyne receivers designed to study spectral lines in the submillimeter-wave region. Finally, a technique for converting the heterodyne radiometer into a spectrometer is described as a means of obtaining line shape details of the 752-GHz H_2O line.

DD FORM 1 JAN 73 1473 EDITION OF 1 NOV 65 IS OBSOLETE

UNCLASSIFIED

SECURITY CLASSIFICATION OF THIS PAGE *(When Data Entered)*